Pretargeting agents and ^{211}At-labeled effector molecules

Synthesis and preclinical evaluation for pretargeted alpha-radioimmunotherapy

Sofia Frost

Department of Radiation Physics
Institute of Clinical Sciences
Sahlgrenska Academy at University of Gothenburg

UNIVERSITY OF GOTHENBURG

Gothenburg 2012

Cover illustration: In the top position of the collage is an α-camera image showing the distribution of ^{211}At in a SAv-MX35-pretargeted tumor at 3 h after the injection of ^{211}At-B-PL$_{suc}$. Below are two SKOV-3 cells pretargeted with trastuzumab conjugated with fluorescence-labeled streptavidin (green) to which poly-L-lysine conjugated with fluorescence-labeled biotin (red) was bound. The structural formula depicts the composition of ^{211}At-B-PL$_{suc}$.

Pretargeting agents and ^{211}At-labeled effector molecules:
Synthesis and preclinical evaluation for pretargeted alpha-radioimmunotherapy

ISBN: 978-91-628-8469-7
E-publication: http://hdl.handle.net/2077/28957
Printed in Sweden by Ineko AB, Gothenburg

Curiouser and curiouser!

Alice in Wonderland, Lewis Carroll

Pretargeting agents and ^{211}At-labeled effector molecules

Synthesis and preclinical evaluation for pretargeted alpha-radioimmunotherapy

Sofia Frost

Department of Radiation Physics, Institute of Clinical Sciences at Sahlgrenska Academy
University of Gothenburg, Gothenburg, Sweden

Abstract

Targeted therapies are treatment regimens in which tumor specific substances incorporating some sort of cell-killing effect are administered to patients. For cancer therapy they have emerged as a means of preventing metastatic relapse by reaching undetected microtumors, thereby improving survival rates. The key to all successful targeted therapy regimens lies in the specificity of the cell-killing effect, i.e. minimizing exposure to normal tissues while maximizing the response in malignant cells. Radioimmunotherapy (RIT) is a targeted treatment modality that utilizes tumor-specific radiolabeled antibodies for the delivery of ionizing radiation to tumors. Although a few RIT regimens have proven effective for certain types of cancer, success is generally limited by unfavorable pharmacokinetics. The large size of antibodies often leads to poor tumor penetration and slow clearance of unbound radioactivity, resulting in insufficient tumor-to-non-tumor absorbed dose ratios.

Pretargeted radioimmunotherapy (PRIT) offers a way of separating the slow targeting phase from the delivery of the radionuclide by using separate molecules for the two stages. In the first step, a modified antibody (pretargeting molecule) is administered and allowed enough time to localize at antigenic sites on tumor cells. Unbound pretargeting molecule is then cleared from the circulation, either spontaneously or with the aid of a clearing agent. Next, a small radiolabeled molecule (effector molecule) with high affinity for the pretargeting molecule is injected. The small size of the effector molecule enables both rapid accretion at pretargeted cells and efficient clearance of unbound radioactivity. With optimization of dosage and timing, very high tumor-to-non-tumor absorbed dose ratios can potentially be achieved using pretargeting.

Different radionuclides can be utilized in targeted therapies depending on their physical and chemical properties. Alpha particle emitters are well suited for irradiation of micrometastases because of their dense ionization and short range in tissue, thereby combining high cytotoxicity to targeted cells with low irradiation of normal tissues. Among the few available alpha-emitters, ^{211}At exhibits promising characteristics in terms of energy emission, decay chain, half-life (7.2 h), and labeling chemistry.

In this work, a pretargeting system utilizing the strong interaction between avidin and biotin was developed and evaluated to determine pharmacokinetics and therapeutic efficacy. Pretargeting molecules were produced by chemical conjugation of (strept)avidin and monoclonal antibodies, and effector molecules were based on biotinylated, charge modified, and ^{211}At-labeled poly-L-lysine. *In vivo* therapy studies in mice were performed using an intraperitoneal model of microscopic ovarian carcinoma, comparing the efficiencies of ^{211}At-PRIT and conventional ^{211}At-RIT. In addition, the pretargeting system was adapted for systemic administration and evaluated in a biodistribution study with mice carrying macroscopic subcutaneous tumors. Proof-of-concept was achieved, with efficient clearance and promising tumor-to-non-tumor absorbed dose ratios for the ^{211}At-labeled poly-L-lysine based effector molecule.

Keywords: Alpha particles, astatine-211, avidin, biotin, ovarian cancer, polylysine, pretargeted radioimmunotherapy

ISBN: 978-91-628-8469-7
E-publication: http://hdl.handle.net/2077/28957

LIST OF PAPERS

This thesis is based on the following papers, which will be referred to by their Roman numerals.

I. Frost SHL, Jensen H, and Lindegren S
In vitro evaluation of avidin antibody pretargeting using ^{211}At-labeled and biotinylated poly-L-lysine as effector molecule
Cancer 2010; 116: 1101–10

II. Frost SHL, Bäck T, Chouin N, Jensen H, Hultborn R, Jacobsson L, and Lindegren S
In vivo distribution of avidin-conjugated MX35 and ^{211}At-labeled, biotinylated poly-L-lysine for pretargeted intraperitoneal α-radioimmunotherapy
Cancer Biother Radiopharm 2011; 26: 727–36

III. Frost SHL, Bäck T, Chouin N, Hultborn R, Jacobsson L, Elgqvist J, Jensen H, Albertsson P, and Lindegren S
Comparison of ^{211}At-PRIT and ^{211}At-RIT of ovarian microtumors in a nude mouse model
Submitted

IV. Frost SHL, Bäck T, Hultborn R, Jacobsson L, Jensen H, Albertsson P, and Lindegren S
In vivo distribution and tumor uptake of ^{211}At-labeled, biotinylated poly-L-lysine for systemic pretargeted radioimmunotherapy
Manuscript

Preliminary results have been presented as follows:

Frost SHL and Lindegren S
In vitro evaluation of avidin antibody pretargeting using ^{211}At-labeled and biotinylated poly-L-lysine as effector molecule

Poster presentation at the 12th Conference on Cancer Therapy with Antibodies and Immunoconjugates, October 16–18, 2008, Parsippany, New Jersey, USA

Poster presentation at the 1st TARCC International Workshop on Targeted Radionuclide Therapy, May 25–26, 2009, Nantes, France

Frost SHL, Bäck T, Jensen H, Hultborn R, Jacobsson L, and Lindegren S
Biodistribution av molekyler avsedda för pretargeted radioimmunoterapi med alfastrålaren ^{211}At

Oral presentation at "Cancerfondens planeringsgrupp för onkologisk nuklidterapi, vårmöte", May 6–7, 2010, Karlstad, Sweden

Frost SHL, Bäck T, Chouin N, Jensen H, Hultborn R, Jacobsson L, and Lindegren S
In vivo distribution of avidin-conjugated MX35 and ^{211}At-labeled, biotinylated poly-L-lysine for pretargeted intraperitoneal α-radioimmunotherapy

Oral presentation at the 7th Symposium on Targeted Alpha Therapy, July 18–19, 2011, Berlin, Germany

Oral presentation at the Oncological Nuclide Therapy Meeting supported by the Swedish Cancer Society, November 16–18, 2011, Uppsala, Sweden

TABLE OF CONTENTS

TERMS AND ABBREVIATIONS

2IT	2-iminothiolane
AES	Affinity enhancement system
AML	Acute myeloid leukemia
ATE	Activated tin ester
Av	Avidin
BMBLR	Bone marrow-to-blood ratio
Bq	Becquerel, SI unit of radioactivity (1 Bq = 1 s^{-1})
bsmAb	Bispecific monoclonal antibody
B/T	Ratio between bound activity and total applied activity
CA	Clearing agent
CEA	Carcinoembryonic antigen
cMORF	Complementary morpholino oligomer
Da	Dalton, SI unit of atomic mass (1 Da = 1 g/mol)
DOTA	1,4,7,10-tetraazacyclododecane-*N*,*N*',*N*'',*N*'''-tetraacetic acid
DSB	Double-strand break
eV	Electron volt, energy unit (1 eV = 1.602×10^{-19} J)
$F(ab')_2$	Antibody fragment
FDA	The U.S. Food and Drug Administration
FPLC	Fast protein liquid chromatography
GFR	Glomerular filtration rate
Gy	Gray, SI unit of absorbed radiation dose (1 Gy = 1 J/kg)
HABA	4'-hydroxyazobenzene-2-carboxylic acid
HAMA	Human anti-mouse antibody
Her2	Human epidermal growth factor receptor 2 (ErbB2)
HGB	Hemoglobin
H&E	Hematoxylin and eosin
IgG	Immunoglobulin G
i.p.	Intraperitoneal
ITLC	Instant thin-layer chromatography
i.v.	Intravenous
K_d	Equilibrium dissociation constant (M)
k_{on}	Association rate constant $([M\cdot s]^{-1})$
LET	Linear energy transfer (keV/µm)
M	Molar, concentration unit (1 M = 1 mol/L)
mAb	Monoclonal antibody
MDS	Multiple damaged sites
MORF	Morpholino oligomer
m-MeATE	*N*-succimidyl-3-(trimethylstannyl)benzoate
MTA	Maximum tolerable activity
MTD	Maximum tolerable dose
MW	Molecular weight

NAGB	Dendrimeric CA containing 16 biotinylated *N*-acetyl-galactosamine residues and a single biotin moiety per molecule
NHL	Non-Hodgkin lymphoma
NHS-LC-biotin	Succinimidyl-6-(biotinamido)hexanoate
NIH:OVCAR-3	Human epithelial ovarian carcinoma cell line
NIS	*N*-iodosuccinimide
PBS	Phosphate buffered saline
p.i.	Post injection
PLT	Platelet
PRIT	Pretargeted radioimmunotherapy
RBE	Relative biologic effectiveness
RBM	Red bone marrow
RCP	Radiochemical purity
RIT	Radioimmunotherapy
RT	Room temperature
SAv	Streptavidin
s.c.	Subcutaneous
SD	Standard deviation
SDS-PAGE	Sodium dodecyl sulfate-polyacrylamide gel electrophoresis
SEM	Standard error of the mean
SKOV-3	Human epithelial ovarian carcinoma cell line
SMCC	Succinimidyl 4-(*N*-maleimidomethyl)cyclohexane-1-carboxylate
SSB	Single-strand break
sulfo-SMCC	4-(*N*-maleimidomethyl)cyclohexane-1-carboxylic acid 3-sulfo-*N*-hydroxysuccinimide ester sodium salt
TFF	Tumor-free fraction
TNBSA	2,4,6-trinitrobenzene sulfonic acid
TNTDR	Tumor-to-normal tissue dose ratio
$t_{½}$	Physical half-life
WBC	White blood cell
%IA/g	Percent of injected activity per gram of tissue

1. INTRODUCTION

1.1 MICROMETASTATIC CANCER

The majority of cancer patients die from metastases rather than their primary tumors. In recent decades, much progress has been made in the field of clinical oncology, but the presence of minimal residual disease still hinders the goal of enhancing survival rates [1]. Despite removal of visible solid tumors and, in many cases, administration of systemic adjuvant treatments, micrometastatic disease results in many patient deaths. The term "micrometastatic" can be applied to tumors of a wide range in size, from single cells to clusters of several millimeters in diameter, their common feature being that they are not identified by conventional markers or imaging techniques. In many cases, early dissemination of cancer cells to secondary sites thus remains concealed at the time of diagnosis and decisions regarding methods for prevention of metastatic relapse must be based on various staging parameters of the primary tumor together with statistical assessments of disease recurrence. Micrometastatic spread is a problem in many common epithelial cancers, such as prostate, breast, and ovarian carcinoma. It has been known for a long time that some cancers metastasize in an organ-specific pattern, and experimental data indicate that the spread is determined by both mechanical factors (how the cells are delivered to the organ) and compatibility factors (molecular interactions between cancer cells and the new organ environment) [2]. Dissemination is thus dependent on inherent features of both the cancer cell and the target organ, and the mutual interaction between these factors.

1.2 TARGETED THERAPY

Already envisioned by Paul Ehrlich in the beginning of the 20th century, "magic bullets" have been realized and implemented to some degree in 21st century medicine [3]. Along with surgery, external radiotherapy, and systemic chemotherapy, targeted therapies have emerged as a means of treating undetected metastases to reduce the incidence of relapse while sparing healthy tissues from negative treatment-related side effects. Targeted therapies are treatment regimens in which a tumor specific substance is administered to the patient, carrying some sort of cell-killing effect – either inherent to the substance or via an additional agent attached to the targeting backbone. Types of inherent effects include blocking the function of signaling molecules/receptors in the target, induction of apoptosis, or indirect action through stimulation of the immune system [4]. Different routes of administration, such as systemic, intracavitary, or oral, can be applied depending on the nature of the disease. The targeting vector should be chosen so as to minimize exposure to normal tissues while delivering a sufficient therapeutic effect to malignant cells. Properties such as size, charge, and biochemical interaction should be taken into careful consideration in order to optimize delivery. The main vectors used for targeting are "small molecules" (non-polymeric organic

compounds of low molecular weight (MW) with high affinity for biopolymers) or antibodies.

Antibodies are molecules that belong to a group of proteins termed immunoglobulins. They consist of four polypeptide chains: two identical light chains and two identical heavy chains, held together by disulphide bridges. Together they form a Y-shaped structure of approximately 155 kDa, containing two antigen binding sites. The true potential of antibodies as targeting vectors became a reality with the development of hybridoma technology in 1975 by Köhler and Milstein [5]. This enabled the isolation of antibodies from a single B-cell clone, allowing for *in vitro* produced monoclonal antibodies (mAbs) with high specificity to their antigen targets. In addition, the hybridoma cell lines can be stored for a long period of time and are able to proliferate indefinitely, thus enabling the production of great quantities of antigen-specific mAbs. In placental mammals immunoglobulins can be differentiated into five antibody isotypes depending on their heavy chains: IgA, IgD, IgE, IgG, and IgM. Through enzymatic digestion the immunoglobulin structure can be split into either two monovalent antigen-binding Fab fragments (55 kDa) and one Fc fragment (using papain) or one bivalent antigen-binding $F(ab')_2$ fragment (105 kDa) and decomposed Fc fragments (using pepsin).

The murine origin of first generation mAbs resulted in limited clinical utility because of issues with immunogenicity and poor interaction with human immune effector cells. After administration of murine antibodies, a human anti-mouse antibody (HAMA) response is common. Adverse reactions are rare, but include allergic reactions towards the murine antibodies that can range from mild (rash) to life-threatening (anaphylactic shock) [6]. In addition, preexisting HAMAs can interfere with the intended therapy by inactivation or complexation with the administered murine mAb leading to altered *in vivo* targeting and distribution. As repeated administrations of mAb may be desired to enhance tumor accretion, immunogenicity becomes an important concern. Advances in protein engineering and library technologies (e.g. phage display [7]) introduced chimeric, humanized, and fully human mAbs, circumventing many of the initial problems [8]. Genetic engineering has further opened up possibilities for designing antibody fragments and fusion proteins such as scFvs (27 kDa), scFv dimers (60 kDa), diabodies (60 kDa), and minibodies (80 kD) [9]. In addition to antibody approaches, another class of low-MW (7 kDa) affinity ligands have been developed using phage display technology, termed affibodies [10]. The size of the antibody fragments determines the rate and route of clearance *in vivo*. Smaller fragments, such as scFvs and diabodies, are removed within a few hours through renal clearance, whereas minibodies and larger molecules stay in the circulation for a longer period of time before clearance via the liver [11]. However, although rapid clearance is beneficial from a toxicity-limiting perspective, it also leads to decreased tumor uptake; these two effects must be balanced in order to achieve successful therapy.

When antibodies or antibody fragments are used unmodified, i.e. as stand-alone treatment, the targeted treatment is referred to as immunotherapy. A few immunotherapy regimens in which the antibody itself mediates the cytotoxic effect have been approved by the U.S. Food and Drug Administration (FDA) and the European Commission, such as rituximab (Rituxan/MabThera) against lymphoma [12], trastuzumab (Herceptin) against breast cancer [13], cetuximab (Erbitux) against colorectal cancer [14], and bevacizumab (Avastin) against various cancers including colorectal, lung, kidney and glioblastomas [15]. In most cases, however, the toxic effect of targeted therapies derives from an attached agent such as a biological toxin, an antineoplastic drug, or a radionuclide [11].

1.2.1 RADIOIMMUNOTHERAPY

Radionuclides can be attached to an antibody-based targeting substance via various labeling methods, directly or using chemical reagents. The cell-killing effect is mediated by ionizing radiation that is emitted by the radionuclide, and the technique is subsequently denoted radioimmunotherapy (RIT). Goldenberg et al. first published experimental results from early RIT experiments with labeled mAbs in 1981 [16]. Since then, a multitude of preclinical and clinical studies have been performed using various types of radionuclides, antibodies, and tumor models [17, 18]. However, unfavorable pharmacokinetics caused by high MW of the antibodies has prevented successful treatment in many cases and reported response rates have been modest. Targeting solid tumors is especially problematic as lymphatic vessels within the tumor often collapse secondary to tumor growth, consequently raising interstitial pressure [19]. As a result, antibody transport into solid tumors is impaired, thereby reducing the delivery of ionizing radiation. On the other hand, RIT has proven more successful for treating hematologic malignancies such as non-Hodgkin lymphoma (NHL), where therapeutic efficacy can be achieved at lower doses and tumor penetration is more feasible [8]. In 2002, Zevalin (^{90}Y-ibritumomab tiuxetan) became the first radioimmunoconjugate to be approved by the FDA for treatment of patients with follicular and transformed NHL [20]. Bexxar (tositumomab and ^{131}I-tositumomab) was FDA approved the following year [21]. In addition to hematologic neoplasms, promising clinical results have been reported from studies of locoregional RIT in patients with minimal residual ovarian cancer (phase I study) and for the treatment of recurrent malignant brain tumors (pilot study) [22, 23]. Currently, the utility of conventional RIT seems greatest in adjuvant settings for treatment of micrometastases or minimal residual disease.

There are five fundamental concerns to address in order to further develop RIT [17]: (i) improved antibody accretion and distribution in tumor tissue; (ii) enhanced clearance of residual non-targeted mAb in blood; (iii) protection of normal tissue from detrimental irradiation; (iv) reduction of mAb-related immunogenicity; and (v) enhanced absorbed dose and dose rate to tumors while minimizing the dose to normal tissue.

1.2.2 PRETARGETED RADIOIMMUNOTHERAPY

An alternative to conventional RIT using labeled mAbs is to separate the targeting phase and the delivery of the radionuclide, physically and temporally. This concept is called pretargeted radioimmunotherapy (PRIT), or simply pretargeting [24, 25]. Several strategies have been presented, all sharing the same fundamental principles (Figure 1): first, a targeting mAb conjugate (pretargeting molecule) is administered and allowed enough time to circulate and specifically bind to tumor-associated antigens. If necessary, circulating unbound mAb conjugate can be removed using a clearing agent (CA). When satisfying tumor-to-non-tumor ratios are achieved, a small radiolabeled molecule (effector molecule) that binds to the localized mAb conjugate is administered, delivering the therapeutic radiation dose. This allows separation of the slow mAb distribution phase from the rapid accretion and clearance of the radionuclide-carrying vector, thereby minimizing systemic irradiation resulting from prolonged circulation of radiolabeled antibodies. The key aspect in all RIT regimens is gaining a balance between the dose delivered to the targeted tumor and exposure of healthy tissue to radiation. In theory, optimization of administration protocols could lead to very high tumor-to-non-tumor ratios using pretargeted strategies.

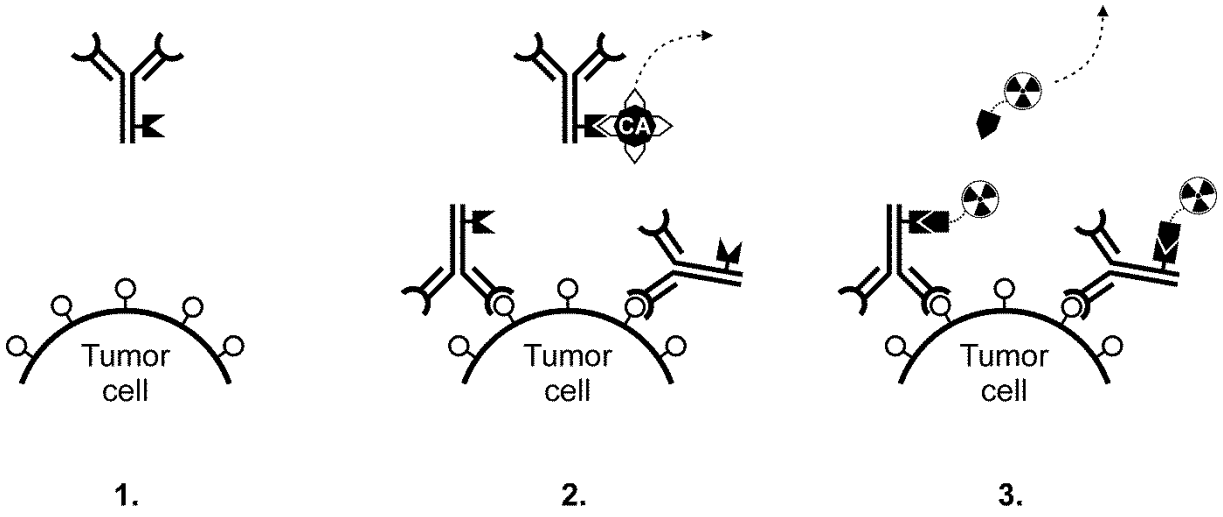

FIGURE 1. Schematic representation of the pretargeting principle. 1) Targeting antibody conjugate (pretargeting molecule) is administered and binds to antigens expressed on the tumor surface. 2) Unbound pretargeting molecule is removed from the circulation, either spontaneously or with the aid of a clearing agent. 3) A radiolabeled vector (effector molecule) is injected and localizes at the pretargeted antigen sites. The small size of the effector molecule facilitates rapid tumor accretion and clearance of unbound radioactivity from blood and normal tissues.

As described earlier, targeting with engineered fragments enables faster clearance, thereby reducing radiation exposure to sensitive normal tissues. At the same time, tumor uptake is decreased, as penetration of macromolecular drugs is a slow process that requires retention in the blood for adequate efficiency. Another factor of importance for delivering therapeutic absorbed doses is tumor residence time, which is reduced with decreasing size of the mAb fragment. With separation of tumor targeting and absorbed dose delivery, as in PRIT, no trade-off concerning these factors is needed.

In 1985, Reardan et al. introduced the idea of separating the radionuclide from the targeting antibody; they proposed that mAbs could be prepared with simultaneous specificity for a tumor-associated antigen and the metal chelate indium-EDTA [26]. Goodwin et al. quickly adapted the technique for tumor imaging with ^{111}In, thereby initiating the pretargeting concept [27, 28]. In current pretargeting strategies, their idea corresponds to the concept of bispecific monoclonal antibodies (bsmAbs) in which antibodies are used with one arm targeting the tumor and the other arm recognizing a radiolabeled ligand [29]. In early studies, the affinity between the bsmAb and the radiolabeled ligand was moderate, and even though the tumor-to-non-tumor tissue contrast ratios were relatively high, tumor uptake was generally low. Le Doussal et al. improved the bsmAb pretargeting system by the application of bivalent haptens to enhance affinity specifically to cell-bound dual specificity antibodies, owing to the formation of cross-linked bsmAb-hapten complexes [30]. This technique was called the affinity enhancement system (AES) and facilitated the combination of high affinity binding to tumor-associated antibodies with reversible monovalent interaction between circulating bsmAbs and radiolabeled haptens [31].

Another PRIT strategy utilizes the strong interaction between (strept)avidin and biotin [32, 33]. Avidin (Av) is a positively charged, glycosylated egg white protein of approximately 66 kDa, with four binding sites for naturally occurring vitamin H (D-biotin). The affinity between avidin and biotin is one of the strongest known non-covalent interactions, with a dissociation constant (K_d) of 10^{-15} M^{-1}. Streptavidin (SAv) is a non-glycosylated analog of avidin produced by *Streptomyces* bacteria with a mass of approximately 60 kDa. It has the same tetravalency for biotin as avidin, but the difference in glycosylation makes the proteins suitable for different applications. Due to the lack of sugar residues, *in vivo* administered streptavidin is retained in the circulation for a longer period of time compared with avidin.

The avidin–biotin system has been used for pretargeting in a number of fashions. In 1987, Hnatowich et al. investigated two approaches for improved imaging: the use of antibodies coupled to either (strept)avidin or biotin in the first step, followed by ^{111}In-labeled biotin or (strept)avidin [34]. Using pharmacokinetic models, Sung and van Osdol concluded that the two-step protocol utilizing streptavidin-conjugated mAbs for targeting and radiolabeled biotin for irradiation was more beneficial than the reverse approach, i.e. biotin-conjugated mAbs and radiolabeled streptavidin [35]. The streptavidin-based effector molecules are currently more or less abandoned, as

radiolabeled biotin derivatives have proved more favorable in terms of clearance, with rapid renal excretion [36]. In Milan, Paganelli et al. first applied the two-step pretargeting protocol using biotinylated mAb MOv18 and ^{111}In-streptavidin in a clinical study with 15 ovarian cancer patients [37]. They concluded that both tumor uptake and tumor-to-normal tissue dose ratios were favorable compared with directly labeled mAbs, both for imaging and therapy. However, an inherent problem with the described two-step approach was that unbound targeting mAbs still remained in the circulation at the time of maximum localization on tumor cells. The Milan group therefore investigated the "chase effect" of avidin in a three-step protocol for tumor detection in patients with increased levels of circulating carcinoembryonic antigen (CEA) [38]. In the first step, biotinylated mAb FO23C5 was administered and allowed to accumulate at the tumor sites. Then, avidin was injected and bound to both tumor-associated and circulating biotinylated FO23C5, the latter fraction being efficiently transported from the blood to the liver. Finally, ^{111}In-biotin was administered and images and biodistribution data were collected. The protocol resulted in improved tumor localization and the method was further refined over the years, adding an injection of streptavidin shortly after the avidin administration for improved targeting. In 1999, the Milan group reported promising therapeutic results from a Phase I/II study conducted in 48 patients with high grade glioma, using ^{90}Y-biotin as the effector molecule [39]. The study was followed a few years later by a non-randomized, 2-arm study with 37 patients, of which 19 were given adjuvant three-step PRIT [40]. Median survival in the treated group was significantly improved compared to the control group, and it was concluded that the technique could be used as part of a combined modality approach and that a randomized trial was justified.

Another three-step PRIT technique using streptavidin and biotin was developed in Seattle. In this approach, tumor cells were pretargeted using a SAv-mAb conjugate followed by a CA before introducing radiolabeled 1,4,7,10-tetraazacyclododecane-*N*,*N*',*N*'',*N*'''-tetraacetic acid (DOTA) biotin in the third and final step. The CA was a biotin-containing galactosylated scavenger molecule that, identical to the avidin chase in the Milan approach, removed remaining mAb conjugate from circulation. Binding of the biotin moiety on the CA to circulating streptavidin-mAb enabled rapid clearance of the pretargeting molecule due to interaction of the galactosamine residues with sugar receptors within the liver. The CA-SAv-mAb complex was subsequently internalized and metabolically degraded. Using the SAv-conjugated mAb NR-LU-10 to target human carcinoma xenografts in nude mice, a more than 20-fold improvement in tumor-to-blood ratios compared with conventional RIT was reported by Axworthy et al. in 2000 [41]. Biotin-galactose-human serum albumin was used as CA before administering ^{90}Y-DOTA-biotin. This was followed by a phase I study with the aim of optimizing the PRIT protocol conducted in 43 patients with adenocarcinomas, showing a ten-fold improvement in tumor-to-bone marrow dose ratio compared with conventional RIT [42]. The protocol was further evaluated and administered to 25 patients with metastatic colon cancer in a phase II trial [43]. Unfortunately, results were disappointing in terms of therapeutic

efficacy (8% overall response rate) and toxicity due to lack of specificity of NR-LU-10 (reactivity with normal gastrointestinal epithelium and renal collecting tubules). The dose-limiting toxicity was diarrhea, but late renal toxicity also occurred in two patients.

However, in spite of unsatisfactory results with NR-LU-10, the Seattle pretargeting strategy was applied to other tumor models and promising results have been reported in the treatment of NHL. Press et al. demonstrated superior biodistribution, reduced toxicity, and enhanced therapeutic efficacy with SAv-conjugated anti-CD20 1F5 mAb compared to directly ^{90}Y-labeled 1F5 for pretargeting of lymphoma xenografts [44]. They used a synthetic CA developed by the NeoRx Corporation (Seattle, WA, USA): biotin-LC-NM-$(GalNac)_{16}$, which contains 16 modified *N*-acetyl-galactosamine residues and one biotin residue per molecule. Their PRIT model was thereafter used in a clinical study of ten patients with CD20-expressing relapsed or refractory NHL, using rituximab as targeting agent [45]. The tumor response was encouraging: seven out of ten patients received a therapeutic dose of ^{90}Y-DOTA-biotin. Of those, six achieved objective tumor regression, including three complete and one partial response. In 2010, Park et al. published results from a comparison between conventional and pretargeted RIT of NHL in mice using the alpha particle emitter ^{213}Bi [46]. The tumors were targeted using an anti-CD20 SAv-1F5$(scFv)_4$ fusion protein and the treatment was well-tolerated with significantly prolonged survival for treated animals. Palanca-Wessels and Press recently summarized results obtained thus far from RIT in NHL, stating among other things that the multistep pretargeting techniques still need to be optimized with regard to timing and dosage of the various administrations, immunogenicity reduction, and choice of radionuclide. Still, they concluded that the great potential with PRIT motivates further clinical trials for the treatment of NHL patients [47].

The Seattle group continued their research and developed their pretargeting system further for use in other tumor models in parallel to NHL. CD45 is a tyrosine phosphatase expressed by most hematologic malignancies, including acute lymphoid and myeloid leukemias. Pagel et al. compared anti-CD20 (1F5) and anti-CD45 (BC8) antibodies for PRIT in nude mice and concluded that both regimens were superior to the directly labeled analogs, but CD45 pretargeting consistently delivered a higher dose to tumors [48]. The anti-CD45 mAb was also more stably retained at the tumor sites. However, in clinical RIT trials using anti-CD45, significant myelosuppression will be an unavoidable problem as most normal hematopoietic progenitor cells express this antigen. Still, encouraging results were obtained when they applied PRIT for the first time in a murine syngeneic myeloid leukemia model; therapeutic absorbed doses of ^{90}Y were selectively delivered to hematopoietic tissues with relatively low accumulation in non-targeted tissues, resulting in significant long-term survival in leukemic mice [49]. The problem of myeloablation remained with this technique, necessitating stem cell rescue for application in clinical trials, but that may be acceptable if survival rates can be improved. The alpha particle emitter ^{213}Bi has been also applied for the treatment of leukemia: Zhang et al. performed preclinical studies of PRIT utilizing ^{213}Bi against adult T-cell leukemia [50, 51], and Pagel et al. recently reported results from further three-step

^{213}Bi-PRIT studies of acute myeloid leukemia (AML) in mice [52]. Tumor localization was rapid and the tumor-to-normal tissue dose ratios were high, yielding excellent tumor regression and improved overall survival compared to the corresponding ^{90}Y-therapy.

A third option for pretargeting is the use of morpholino-oligonucleotides and complementary nucleic acid sequences [53, 54]. This strategy was introduced by Kuijpers et al. in 1993 via hybridization of complementary DNA fragments (oligonucleotides) that could be used for recognition between a radionuclide and pretargeted tumor cells [55]. Their pretargeting concept was based on administering an antibody-oligonucleotide conjugate in the first step, which was targeted by radiolabeled antisense nucleotide in the second step. The methodology was refined by replacing the phosphate-ribose backbone of the DNA by a polyamide backbone, resulting in a peptide nucleic acid that was shown to be more useful for pretargeting because of better stability, high binding affinity to their complement, and improved pharmacokinetics [56]. Further enhancements were reported as researchers moved on to using morpholino oligomers (MORFs), which are commercially available synthetic DNA analogs with high specificity towards their complementary MORFs (cMORFs) [57]. Liu et al. evaluated this system in mice using the anti-CEA antibody MN14 conjugated to an 18-mer MORF and its ^{99m}Tc-labeled cMORF [58]. They reported rapid pharmacokinetics with good tumor uptake and low normal tissue uptake, except for the kidneys, which showed some accumulation of radioactivity. The technique was also successfully applied to androgen-dependent prostate cancer xenografts in mice, albeit with lower tumor accumulation than expected [59]. He et al. showed that target localization of radioactivity could be improved using amplification targeting, a multistep procedure in which a polymer conjugated with multiple copies of cMORF is administered between the antibody-conjugated MORF and a radiolabeled MORF [54]. Preliminary studies of this affinity enhancement demonstrated the feasibility of synthesizing bivalent MORF effectors and that bimolecular binding could be achieved, resulting in a lower dissociation rate constant and higher affinities for the bivalent MORFs compared to that of their monovalent forms [60, 61].

In 2001, Chmura et al. proposed a pretargeting model under development, which uses the approach of producing engineered antibody–ligand binding pairs with even greater affinity than the avidin–biotin system [62]. Infinite affinity binding was achieved by altering the binding sites of the antibody and the ligand, enabling covalent reaction, thereby eliminating dissociation of the binding pair. The system is still in its infancy, but promising results from a study of PET imaging of reporter genes using an antibody fragment with infinite binding to an yttrium-labeled reporter probe have been published [63].

1.3 Radionuclides for Targeted Therapy

The choice of radionuclide for use in targeted therapy depends on both physical and chemical properties. Mode of decay, physical half-life ($t_{½}$), and decay chain should be carefully considered, and so must the possibility of creating stable chemical conjugates with appropriate carrier molecules. Biological concern must also be considered with regard to the fate of the radionuclide following metabolism of the radiolabeled vector. Ultimately, a prerequisite for the use of any radionuclide that fulfills the stated criteria is availability: a condition that in many cases turns out to be the most difficult to meet.

To achieve therapeutic response from ionizing radiation, sufficient energy must be deposited in the tumor. With higher doses more cells will be killed and the probability of damaging the target tissue is increased. The ionization density after the transit of a charged particle through matter can be described by the linear energy transfer (LET). It is expressed in keV/μm and reflects the energy absorbed in matter per unit path length traveled by a charged particle. For a particular material, the LET values of particles of equal energy increase as follows: high energy electrons < beta particles < protons < alpha particles < heavy ions < fission fragments. Biologic effects from irradiation arise mainly from DNA damage, which can be the result of either direct ionization or through interaction with radiation-induced free radicals. Different DNA lesions can occur, such as single-strand breaks (SSBs), double-strand breaks (DSBs), or multiple damaged sites (MDSs) that involve several types of lesions in close proximity to each other. Many DNA lesions are repaired efficiently, except for DSBs and MDSs, which are complex and thus more prone to result in cell death. Sparsely ionizing (i.e. low-LET) radiation is more likely to generate sublethal damage such as reparable SSBs, whereas the frequency of DSBs has been observed to increase with LET [64]. In addition, the lethality of the DSBs increases with the LET up to approximately 300 keV/μm after which it decreases for very heavy ions [65]. Practically, this means that it takes several thousands of low-LET particle traversals through the nucleus to kill a mammalian cell, compared to only 1–50 for high-LET [66, 67].

Another factor influencing cell survival is dose rate, but this is mainly important for low-LET radiation. The biological response is affected by the physical as well as the biological half-life, meaning that treatments using radioimmunoconjugates with infinite residence time at the target will benefit from a long physical half-life. However, higher dose rates delivered during shorter times are more effective from a radiobiological perspective. Consequently, the biological effects from short-lived radionuclides will be greater than those resulting from therapy using nuclides with similar emission energy and longer half-life [66]. Furthermore, the presence of oxygen makes mammalian cells more sensitive to radiation, as it promotes the formation of free radicals. The oxygen effect is important for low-LET irradiation but negligible for high-LET, meaning that high-LET emitters also allow effective cell-killing under hypoxic conditions [68].

1.3.1 Beta Particle Emitters

Electrons or positrons that are emitted from the nuclei of unstable elements are called beta particles (β). They have various ranges in tissue depending on their energy (0.05–2.3 MeV), the maximum being around 1 cm [66]. Their mean LET is low, only approximately 0.2 keV/μm. Due to the long range, all cells within a tumor do not have to be targeted as long as they are close enough to the decaying radionuclides; this effect is called cross-fire.

Historically, the most studied radionuclides in RIT are β-emitters: ^{131}I and ^{90}Y. In addition to the β-particles, ^{131}I ($t_{½}$ = 8.0 d) co-emits γ-radiation that is suitable for imaging. Being readily available, inexpensive, and offering feasible protein labeling chemistry, ^{131}I has been used in many clinical trials. ^{90}Y ($t_{½}$ = 64.1 h) is a pure β-emitter and thereby more favorable than ^{131}I in terms of radiation protection. The β-particle energy is higher for ^{90}Y (maximum energy 2 280 keV for ^{90}Y; 610 keV for ^{131}I) which leads to longer particle range *in vivo* (maximum particle range 12 mm for ^{90}Y; 2 mm for ^{131}I), making it less appropriate for irradiation of smaller tumors. ^{90}Y-labeling of antibodies is generally performed using DOTA, a chelator known to form stable labels with metals, an important feature as ^{90}Y accretes in bone if released from the targeting mAb [69].

1.3.2 Alpha Particle Emitters

Alpha particles (α) consist of two protons and two neutrons, thus having a mass and charge (+2) that is equal to that of a helium nucleus. The energy delivered by α-emitters is in the range of 5–9 MeV in just 40–100 μm [66], leading to LET values in the range of 50–230 keV/μm [67]. This causes extensive ionization in matter, making them far more cytotoxic than β-emitters. The difference in cytotoxicity can be described in terms of relative biologic effectiveness (RBE), which is a measurement of the effect from equal absorbed doses of different types of radiation. Due to their short range *in vivo*, α-emitters are well suited for irradiation of micrometastases and circulating tumor cells (e.g. hematologic malignancies).

Unfortunately, the list of potentially useful α-emitting radionuclides for targeted therapies is not long. Currently, it includes ^{149}Tb, ^{211}At, ^{212}Bi, ^{213}Bi, ^{223}Ra, ^{224}Ra, ^{225}Ac, ^{226}Th, ^{227}Th, and ^{255}Fm [70]. Some of the listed nuclides are very difficult to produce (^{149}Tb and ^{255}Fm) and some have α-emitting daughters with long enough half-lives to redistribute and decay outside the target (^{223}Ra, ^{224}Ra, ^{225}Ac, ^{226}Th, ^{227}Th) making them less useful. The most interesting α-emitting radionuclides are at present ^{212}Bi ($t_{½}$ = 60.6 min), ^{213}Bi ($t_{½}$ = 45.6 min), and ^{211}At ($t_{½}$ = 7.2 h), with average α-particle energies ranging from 6.8 to 8.3 MeV [71]. Their daughters have short half-lives and their production is feasible; the two metallic bismuth isotopes are eluted from ^{224}Ra and ^{225}Ac generators, whereas the halogen ^{211}At is cyclotron-produced [72-74]. However, their short half-lives place high demands on the labeling techniques, as lengthy procedures can result in poor radiochemical yields despite high chemical yields because of decay during labeling and purification.

1.3.3 Combination Treatments

For every radionuclide there exists a range of tumor sizes in which treatment can be efficient [75]. In the clinical situation, however, patients with disseminated disease often display a variety of tumor sizes. Together with the fact that the distribution of radiolabeled vectors is often far from uniform, this implies that the use of a number of radionuclides simultaneously could be more beneficial than using merely one. A long-range emitter such as ^{90}Y could, for instance, be used together with a short-range emitter like ^{211}At; cross-fire would then help to overcome issues from heterogeneous distribution, and the core of larger tumors could be reached while still enabling delivery of high energy to small tumor clusters and micrometastases.

2. AIMS

The overall aim of this PhD project was to evaluate a system for pretargeted alpha-radioimmunotherapy of disseminated cancer. The main objective was to investigate whether the developed pretargeting system would be equal to, or better than, conventional alpha-radioimmunotherapy. The studies have covered several aspects including design and synthesis of pretargeting and effector molecules.

Specific aims of the separate studies included in the thesis were:

- to synthesize and evaluate avidin-coupled monoclonal antibodies together with a poly-L-lysine based, biotinylated, succinylated, and ^{211}At-labeled effector molecule in an *in vitro* model (Paper I);
- to separately evaluate the developed substances in an *in vivo* mouse model with regard to biodistribution and toxicity after intraperitoneal injections (Paper II);
- to compare the therapeutic efficacy and toxicity of the developed intraperitoneal pretargeting system with that of conventional ^{211}At-radioimmunotherapy for treatment of ovarian microtumors in mice (Paper III); and
- to assess the potential of the developed pretargeting system for systemic therapy in comparison to conventional ^{211}At-radioimmunotherapy with regard to biodistribution and toxicity after intravenous injections (Paper IV).

3. ASTATINE-211

3.1 GENERAL

Astatine-211 decays with a $t_{½}$ of 7.2 h in two branches, ultimately resulting in 100% α-emission (Figure 2). The first branch has 58% probability of occurring: disintegration through electron capture to ^{211}Po, which rapidly ($t_{½}$=0.52 s) decays to stable ^{207}Pb through α-particle emission (7.45 MeV). Consequently, the other branch has 42% probability of occurring: α-particle emission (5.87 MeV) to ^{207}Bi, which eventually ends in ^{207}Pb via electron capture ($t_{½}$=38 y). Quantification of the ^{211}At-activity is enabled by the X-ray photons (77–92 keV) emitted following the electron capture to ^{211}Po.

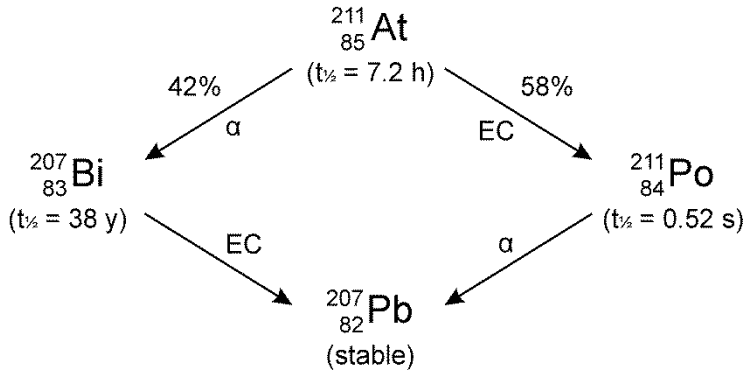

FIGURE 2. Simplified scheme of the branched ^{211}At decay. EC = electron capture.

A number of nuclear reactions can be utilized for producing ^{211}At, but for routine production the most commonly used method is α-particle bombardment of metallic bismuth through the ^{209}Bi(α,2n)^{211}At reaction [76]. This can be achieved using cyclotron beam irradiation with incident α-particle energy ($E_α$) of 20–31 MeV, the optimum being approximately 28 MeV. Higher $E_α$ leads to significant contamination by the isotope ^{210}At, which is produced in the competing ^{209}Bi(α,3n)^{210}At reaction and decays into the highly toxic α-emitter ^{210}Po.

The ^{211}At can be separated from the irradiated bismuth target through dry-distillation or via acid treatment of the target followed by solvent extraction. The main approach is dry-distillation in chambers of various dimensions depending on the size of the cyclotron target, with the temperature being in the range of 650–800°C. The ^{211}At used for experiments described in this thesis was produced by the Cyclotron and PET Unit, Rigshospitalet (Copenhagen, Denmark) and recovered after transportation of the irradiated target to Gothenburg using a dry-distillation procedure introduced by Wilbur et al. [77] and further developed by Lindegren et al. [78]. Briefly, the irradiated bismuth layer was mechanically removed from the target backing plate and carefully transferred

to a cylindrical quartz vessel, which was inserted in a still (quartz tube) placed in a tube furnace preheated to 670°C. Vaporized ^{211}At was transported from the still by promptly reducing the pressure on the outlet side, and trapped by condensation in a cooled (–77°C) capillary loop. The captured ^{211}At was recovered by rinsing the capillary tube with a small volume of chloroform. The chloroform was subsequently evaporated under gentle nitrogen flow before labeling, leaving a dry astatine residue in the vial.

3.2 Astatine Labeling

Astatine is the heaviest element in the halogen group in the periodic table of the elements. It shares many chemical properties with other halogens, such as iodine, which is the most studied radionuclide regarding protein labeling. The main procedure for binding radioiodine to proteins is generally referred to as "direct" labeling, and involves reaction of oxidized (electrophilic) iodine (I^+) with tyrosine groups on the protein. However, even though this labeling technique works for iodine, it cannot be readily translated for direct labeling with other radiohalogens. Although proteins can be labeled with astatine through direct electrophilic reactions, the yields are generally low and the products have displayed poor stability, probably due to nonspecific weaker bonds caused by a difference in the oxidation state of astatine compared to iodine [79]. Stability is of key importance when working with ^{211}At-labeled radiopharmaceuticals because of the high cytotoxicity of α-emitters, which disqualifies this kind of direct astatination. Stably radioiodinated compounds are often used as internal controls for studying the stability of ^{211}At-labeled vectors, because of differences in normal organ uptake of released iodine and astatine. Both radionuclides accumulate in the stomach and thyroid, but free astatine also exhibits elevated levels in the lung and spleen. Co-injection of an ^{125}I- or ^{131}I-labeled compound with the same ^{211}At-labeled compound thus reveals unwanted deastatination and facilitates analysis of astatinated products.

Another option for radiohalogenation is conjugate labeling, i.e. labeling of proteins via conjugation with radiolabeled small molecules (reagents), a concept that Wilbur thoroughly reviewed [80]. Despite the fact that astatine belongs to the halogens, it displays some metal-like characteristics that has motivated labeling studies using chelating agents such as DOTA [70]. Already in 1940, Corson et al. stated that the chemical behavior of astatine – simply called "element 85" at the time – was generally that of a metal [81]. Results achieved to date by the chelation approach to ^{211}At-labeling support further studies, but it is uncertain as to whether the approach will be practically useful for labeling of biomolecules.

Hypothesizing that the carbon–halogen bond may be too weak for sufficient *in vivo* stability, Wilbur et al. studied a number of new reagents for direct astatination of proteins based on boron–halogen bonding [82, 83]. Their *closo*-decaborate(2–) cage enables direct astatination with high labeling yields and decreased deastatination *in vivo*, also for small or rapidly metabolized targeting agents. However, the negatively

charged moiety shows some retention in liver and kidneys necessitating further modifications.

Despite the deastatination concerns, the most utilized approach for producing ^{211}At-labeled proteins is a two-step labeling using bifunctional agents that are radiolabeled in the first step and then conjugated to the ε-amine of lysine within a protein in the second step. Aryl-tin *N*-succinimidyl ester derivatives, referred to as activated tin ester (ATE) reagents, have been developed to take advantage of the suitable properties of tin–carbon groups in electrophilic halogenation reactions [84-86]. High labeling yields (>90%) of the small molecules in the first step have been reached using aryl stannyl intermediates, through the formation of an aryl-carbon–astatine bond. After protein conjugation, the overall astatination yields have been in the order of 50%, because of competing hydrolysis of the active ester [70]. To reduce the activity loss due to decay and work up, and minimize potentially deteriorative radiolysis effects from lengthy labeling reaction times, a direct one-step procedure for astatination of proteins was developed in our lab [87]. Antibodies were conjugated with *N*-succinimidyl-3-(trimethylstannyl)benzoate (m-MeATE) and the immunoconjugate subsequently labeled with ^{211}At. The ^{211}At-labeling was completed almost instantaneously with high radiolabeling yields (60–80%), even at low antibody conjugate concentrations. The purity and stability of the resulting ^{211}At-labeled antibody was good, with only minor differences in tissue uptake compared with conventionally two-step labeled antibodies. This direct astatination procedure has successfully been applied for ^{211}At-labeling of F(ab')$_2$ fragments intraperitoneally (i.p.) administered to patients with recurrent ovarian carcinoma (unpublished). In Paper I, the one-step procedure was adapted for ^{211}At-labeling of poly-L-lysine-based effector molecules, as described in section 5 of this thesis.

4. OVARIAN CANCER

4.1 THERAPEUTIC CONSIDERATIONS

Ovarian cancer is a disease with late and unspecific symptoms, resulting in a poor prognosis. In a majority of patients, tumors have spread outside the ovaries to the peritoneal cavity and lining (stage III) at the time of diagnosis. Relapse is common, in spite of apparently complete clinical remissions. The main route for dissemination is the movement of detached malignant cells from the ovaries directly to the abdominal cavity, where they form micrometastases on the peritoneal surface [88]. In stage III ovarian cancer, retroperitoneal lymph nodes are frequently affected but seem to respond well to chemotherapy. The pattern of recurrence is dominated by relapses within the peritoneal cavity, making an i.p. treatment modality desirable. Metastases to other distant organs at diagnosis are possible, but at that stage (stage IV) no cure can be achieved. A conceivable strategy for stage III ovarian cancer would be to initiate consolidating treatment of possible micrometastases at a point in time when the tumor burden is minimal, i.e. following cytoreductive surgery and chemotherapy. After a number of preclinical studies of ^{211}At-RIT demonstrating therapeutic potential [89-95], a clinical Phase I trial with i.p. administered ^{211}At-labeled MX35 F(ab')$_2$ fragments was launched in 2005, including nine women seemingly in complete remission following salvage chemotherapy after i.p. relapse [22]. The collected pharmacokinetic data, the lack of objective (myelotoxicity, i.e. suppression of white blood cells and platelets) and subjective (e.g. fatigue, nausea, pain) side effects, and the very low absorbed dose to bone marrow indicated that potentially therapeutic absorbed doses may be delivered using that system.

However, preclinical studies showed that tumors larger than approximately 0.1 mm in diameter were less curable with conventional ^{211}At-RIT [92, 93]. This could be due to insufficient penetration of radiolabeled antibodies into the tumor volume; the use of a pretargeting strategy may therefore improve the radioactivity distribution, as discussed in the introduction of this thesis. In Papers I–III, a pretargeting system for i.p. ^{211}At-PRIT of ovarian microtumors was developed and investigated through *in vitro* cell assays and *in vivo* studies of biodistribution and therapeutic efficacy. In Paper IV, the pretargeting system was adapted to systemic conditions and evaluated in a subcutaneous (s.c.) ovarian tumor model.

4.2 TUMOR MODEL

In all kinds of targeted therapies, the ability to discriminate between normal and malignant cells is of paramount importance, and the targeting vector must be chosen with regard to high specificity for tumor associated antigens. For PRIT, another particularly important trait of the tumor localizing mAb is the residence time on the cell surface, as it must remain available when the effector molecule is administered. Hence, after binding to the antigens the pretargeting molecule must neither be internalized by the tumor cells nor shed from the cell surface prior to injection of the radiolabeled

effector molecule. The work described in this thesis has been based upon two antibody/antigen models that fulfill these criteria: trastuzumab/SKOV-3 and MX35/NIH:OVCAR-3. The *in vitro* system developed in Paper I utilized trastuzumab as the targeting agent, while the animal studies in Papers II–IV were performed using MX35. Trastuzumab is a commercially available humanized IgG mAb with high affinity for the extracellular domain of the human epidermal growth factor ErbB2 (Her2). ErbB2 is overexpressed in 20–30% of epithelial ovarian cancer tumors, depending on disease stage [96]. MX35 is a murine IgG mAb that recognizes the membrane transporter protein NaPi2B, which is homogeneously expressed on approximately 90% of human epithelial ovarian cancers [97]. The MX35 hybridoma was obtained from the Ludwig Institute for Cancer Research (New York, NY, USA) and cultured at the Department of Cell and Molecular Biology at the University of Gothenburg.

Both SKOV-3 and NIH:OVCAR-3 are human epithelial ovarian carcinoma cell lines, acquired from the American Type Culture Collection (ATCC; Rockville, MD, USA) and cultured at the Department of Oncology at Sahlgrenska University Hospital (Gothenburg, Sweden). The antigen expressions of the two cell lines have previously been assessed using Scatchard analysis, resulting in approximately 1.5×10^6 antigenic sites sites/cell for trastuzumab/SKOV-3 [98] and 1.2×10^6 for MX35/NIH:OVCAR-3 [93]. In addition, the association rate constant k_{on} was estimated to be 80 000 and 66 000 $[M\cdot s]^{-1}$ for SKOV-3 and NIH:OVCAR-3, respectively. After i.p. inoculation of NIH:OVCAR-3 cells, the tumor growth mimics human disease, with peritoneal carcinomatosis and production of ascites (pathological accumulation of fluid in the peritoneal cavity) [99].

5. PRETARGETING SYSTEM

All pretargeting systems described in the introduction have their benefits and disadvantages, and it is not yet determined which is the most suitable for delivering ^{211}At to tumor cells. The bsmAb system, the use of MORFs/cMORFs, and infinite affinity binding all show promise for therapeutic applications, but further development of the astatination chemistry is required for ^{211}At-labeling of the divalent haptens and other effector molecules. For the avidin–biotin system, the process of developing ^{211}At-carriers is currently more advanced and a number of molecules have been evaluated in preclinical studies. We therefore chose to base our pretargeting model on avidin–biotin interaction, and the development is described in Paper I.

5.1 PRETARGETING MOLECULE

5.1.1 AVIDIN-ANTIBODY CONJUGATION

Avidin and streptavidin can be coupled to mAbs in a number of ways, which can be summarized as i) biochemical cross-linking, ii) chemical conjugation, or iii) genetic fusion. Biochemical coupling utilizes biotin as a link between avidin and antibody, and can be easily achieved using biotinylation reagents for coupling of the vitamin to lysine residues on the mAb. A disadvantage of this technique is that one of the four binding sites for biotin is consumed by the linkage to the biotinylated mAb, consequently reducing the avidity of the pretargeting molecule. The use of bifunctional chemical reagents avoids this problem by sustaining the multivalency of (strept)avidin for biotin. Chemical conjugation methods exploit the sulfhydryl (–SH) groups introduced on the antibody either by reduction of existing disulfide bridges or by addition of thiols on lysine residues. The former can been performed using (2-mercaptoethyl)amine (MEA) or dithiothreitol (DTT), whilst 2-iminothiolane (2IT) is frequently used in the latter case [100-103]. The thiolated mAbs can readily react with maleimide-bound (strept)avidin, forming stable carbon–sulfur (amide–thioeter) bonds. The maleimides are loaded onto the (strept)avidin primarily using the bifunctional reagent succinimidyl 4-(*N*-maleimidomethyl)cyclohexane-1-carboxylate (SMCC).

The biochemical and chemical methods are robust and feasible, but there are several drawbacks. Using biochemical conjugation, the tetravalency of (strept)avidin enables the formation of unwanted dimeric and polymeric (S)Av-mAbs consisting of several antibodies joined together, which necessitates purification of the product to isolate the desired monomer fraction. Removal of high MW cross-linked species is also required after chemical conjugation, lowering the overall product yield of monomeric (S)Av-mAb. An additional problem related to thiolation of antibodies using 2IT is the limited control of site-specific modification; the alterations are distributed randomly on the antibody framework without discrimination of antigen-binding regions. Conjugation of (strept)avidin at sites close to, or directly involved in, antigen-binding may lead to reduced immunoreactivity, negatively affecting tumor targeting. Genetically engineered

fusion proteins are superior in terms of immunoreactive integrity and product homogeneity. With a suitable expression system they can be manufactured cost-efficiently in large quantities, but the development of appropriate systems is generally difficult and time-consuming. Chemically synthesized conjugates may therefore be preferable for the development of prospective pretargeting systems, and as a convenient aid in designing optimal fusion proteins.

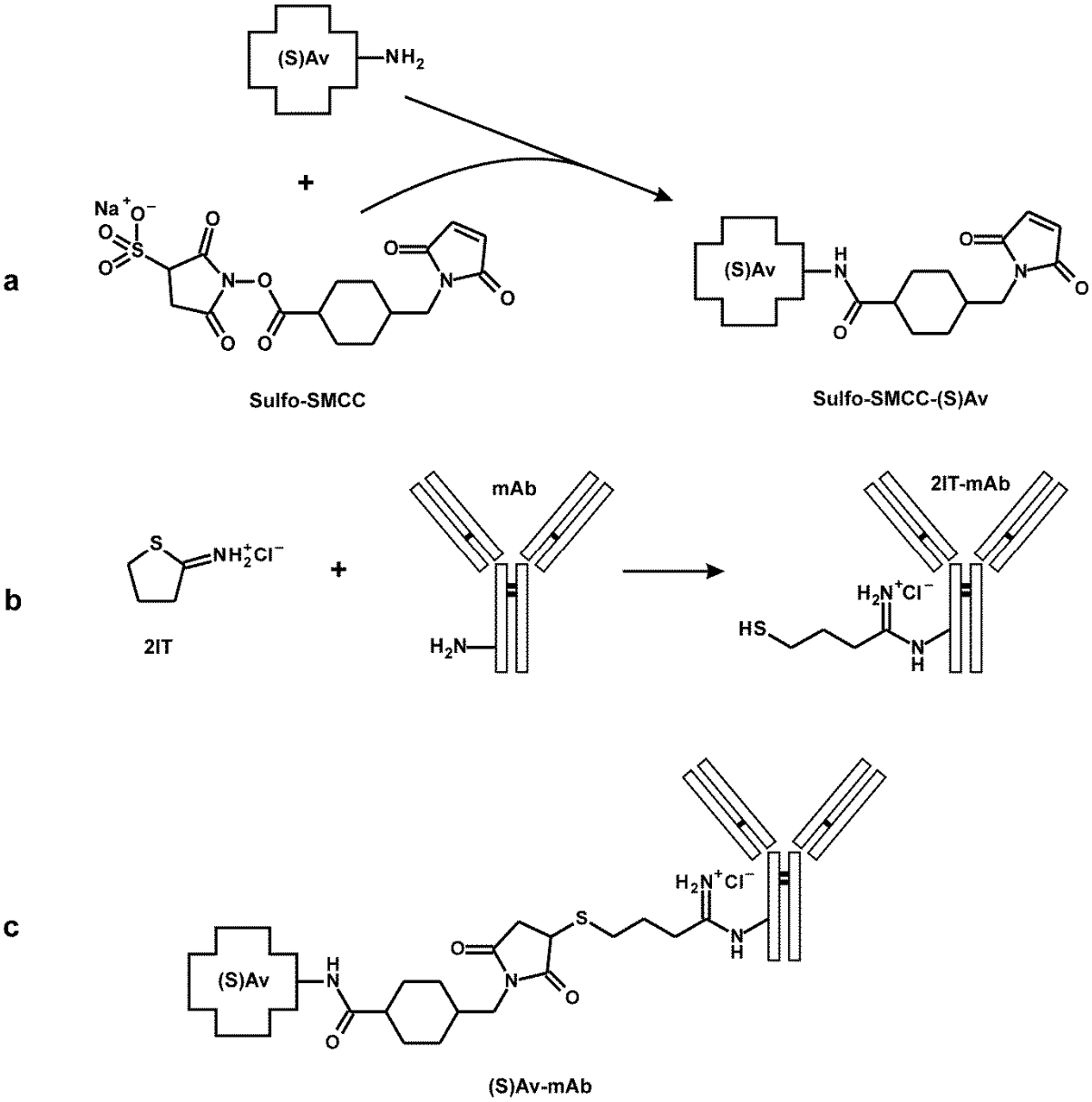

FIGURE 3. Schematic overview of the conjugation of (strept)avidin to antibodies. a) Activation of (S)Av using sulfo-SMCC, b) thiolation of mAb using 2IT, c) the resulting (S)Av-mAb conjugate.

Paper I describes the chemical conjugation method used to produce (strept)avidin-coupled mAbs in this project. Avidin was activated by addition of a ten-fold molar excess of 4-(*N*-maleimidomethyl)cyclohexane-1-carboxylic acid 3-sulfo-*N*-hydroxysuccinimide ester sodium salt (sulfo-SMCC), and incubated at room temperature (RT) for 30–60 min. Trastuzumab was thiolated by reaction with 10–20-fold molar excess of 2IT for 30–60 min at RT. Sulfo-SMCC-Av and thiolated trastuzumab were purified separately by gel filtration using a prepacked Sephadex™ G-25 column, before being mixed at an equimolar ratio and incubated overnight at 4°C. The resulting Av-trastuzumab monomer fraction was isolated from unreacted mAb and higher MW cross-linked species by size exclusion fast protein liquid chromatography (FPLC) and iminobiotin affinity chromatography. Figure 3 depicts the reaction scheme.

Because we aimed for i.p. PRIT studies initially (Papers II and III), the *in vitro* model was based on an avidin-conjugated pretargeting molecule. The hypothesis was that the use of avidin would eliminate the need for an additional CA, as unbound Av-mAb would be rapidly directed to the liver. For systemic applications (Paper IV) avidin was interchanged for the non-glycosylated streptavidin, using the same conjugation protocol.

5.1.2 Characterization of the Avidin-Trastuzumab Conjugate

The MW of the purified avidin-trastuzumab conjugate was estimated using sodium dodecyl sulfate-polyacrylamide gel electrophoresis (SDS-PAGE). In order to assess the immunoreactivity, i.e. cell binding, and the biotin-binding ability of the Av-trastuzumab pretargeting molecule, the conjugate was ^{211}At-labeled according to the one-step procedure described previously [87]. The biotin-binding capacity was determined by incubation with immobilized iminobiotin, and the binding to cells was assessed through the use of an *in vitro* cell assay, developed from the Lindmo assay [104]. SKOV-3 cells in single-cell suspension (5×10^6 cells/mL) were serially diluted 1:2 five times, yielding six different concentrations. An equal amount of radiolabeled pretargeting molecule was added to all tubes and the cells were incubated at RT during gentle agitation for 2 h. The unbound activity was washed off and the cell-associated radioactivity was measured in a gamma counter. Cell binding was then determined from the ratio between bound activity and total applied activity (B/T) for each dilution. B/T was plotted against cell concentration, and the shape of the curve revealed whether saturation was reached or not; for a saturated assay the B/T ratio reached a plateau corresponding to the immunoreactivity of the labeled pretargeting molecule.

5.2 Effector Molecule

5.2.1 Synthesis

The principal features of the radiolabeled effector molecule should be rapid accumulation at pretargeted tumor sites and short retention in blood and normal tissues, preferably with renal clearance. Most of the work with biotin-effectors has been performed by radiolabeling of a number of biotin derivatives, but investigations using ^{211}At has been hampered by the low availability of the radionuclide. Foulon et al. performed the first astatination of a biotin derivative for PRIT in 1997 [105]. Since then, Wilbur and co-workers have explored the field, focusing particularly on stability of ^{211}At-labeled products, as *in vivo* deastatination is commonly seen for rapidly metabolized targeting agents [106, 107].

In 1987, Torchilin et al. introduced the idea of increasing the specific activity of radiolabeled antibodies for imaging using chelate-modified polymers that preserved the antigen-binding ability [108]. A few years later, del Rosario and Wahl further developed the concept by using a small radiolabeled peptide (poly-L-lysine) with multiple biotins for localization of pretargeted streptavidin [109]. This opened up possibilities for improvement of the *in vivo* targeting and increasing the delivered dose to tumors, as the polymer exhibits multiple ε-amino groups that are available for *N*-acylation reagents. Bifunctionate conjugates with multiple biotins as well as intermediate reagents or chelates for radiolabeling can thus be produced, subsequently raising both the avidity and specific activity of the effector molecule. Moreover, the use of a polymeric backbone allows increased control over the *in vivo* distribution, as peptides of different MW can be chosen. Compared with biotin, which displays very short retention in circulation, the biotinylated peptide is allowed greater opportunity for binding interaction due to slower clearance. Biotinylated, astatinated, and succinylated poly-L-lysine conjugates of different sizes (13, 38, and 363 kDa) for PRIT were prepared by Lindegren et al., showing different clearance rates and routes after i.p. administration, the smallest being rapidly excreted through renal clearance [110]. A comparison between polylysine L- and D-isomers was also performed, showing a striking difference in whole-body retention between the two, and high renal uptake of the D-isomer [111].

In Paper I, the synthesis of a biotinylated, ^{211}At-labeled, and succinylated poly-L-lysine (^{211}At-B-PL$_{suc}$) conjugate is described. Because the aim was to construct a model pretargeting system for *in vitro* proof-of-principle, a large poly-L-lysine backbone (MW approximately 130 kDa) could be chosen in order to simplify conjugation and purification. Poly-L-lysine in 0.2 M carbonate buffer (pH 8.5) was incubated with a ten-fold molar excess of succinimidyl-6-(biotinamido)hexanoate (EZ-link NHS-LC-biotin) reagent at RT for 30 min, after which m-MeATE was added. After an additional 30 min, the biotinylated and m-MeATE-conjugated polymer was isolated in 0.2 M sodium acetate buffer (pH 5.5). Astatination of the conjugate was then performed: NIS in methanol/1% acetic acid was added to oxidize the dry astatine residue, followed by addition of the biotinylated m-MeATE-poly-L-lysine conjugate and reaction for 1 min. NIS was then

added and the reaction mix incubated for 1 min. Unmodified amino groups in poly-L-lysine are readily protonated resulting in a positively charged molecule that exhibits a high degree of nonspecific binding both *in vitro* and *in vivo*. Under these conditions, only a small fraction of the total amount of amino groups is substituted by biotinylation and radiolabeling, and succinic acid was therefore added to charge modify the molecule by conversion of the remaining amino groups to succinic acid residues. After a 15-min succinylation reaction, the ^{211}At-B-PL$_{suc}$ product was isolated using a prepacked Sephadex™ G-25 column.

In Papers II–IV, the 130 kDa poly-L-lysine base was exchanged for a smaller peptide of high purity and well-defined size (30 lysine residues, MW 3865 Da). In addition, the NHS-LC-biotin reagent was substituted by NHS-dPEG®$_4$-biotinidase resistant biotin for improved serum stability *in vivo*. The synthesis of ^{211}At-B-PL$_{suc}$ was further refined by reversing the order of radiolabeling and succinylation. By doing so, the biotinylated, m-MeATE-conjugated, succinylated reagent (m-MeATE-B-PL$_{suc}$) could be prepared in advance, generally the day before astatination, thereby reducing the time needed for ^{211}At-labeling, which is a great benefit given the 7.2 h half-life of ^{211}At. Figure 4 depicts the synthesis of the ^{211}At-B-PL$_{suc}$ effector molecule used in Papers II–IV.

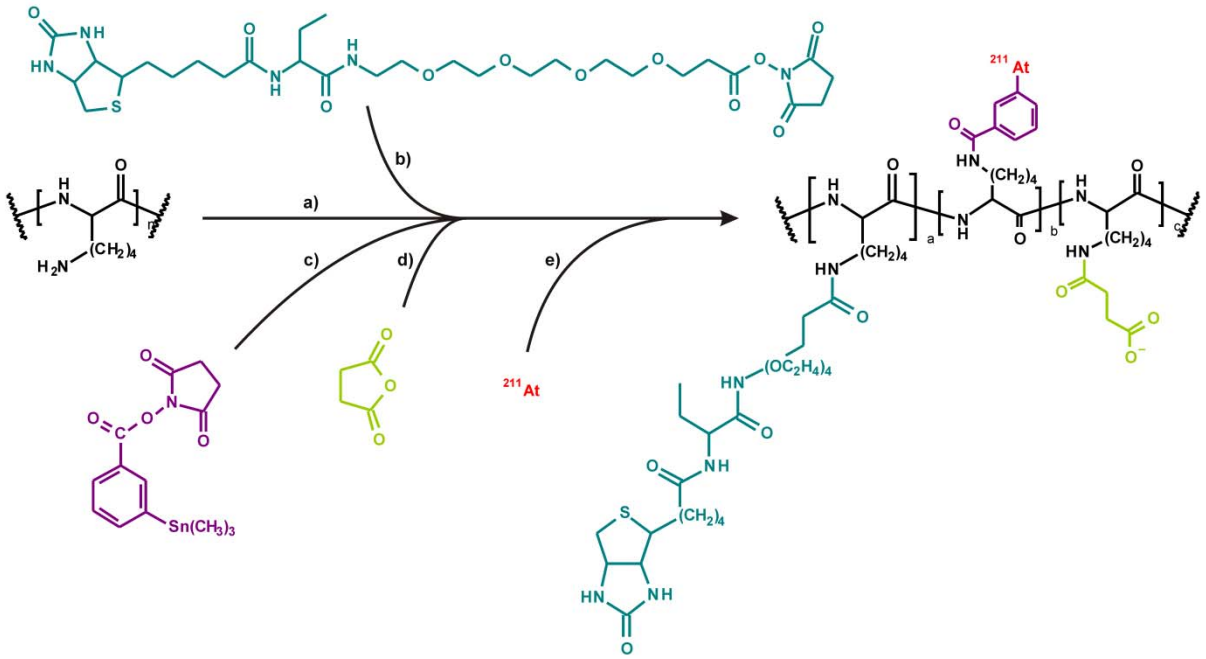

FIGURE 4. General scheme for the synthesis of biotinylated, succinylated, and ^{211}At-labeled poly-L-lysine (^{211}At-B-PL$_{suc}$). a) Poly-L-lysine, b) biotinylation using NHS-dPEG®$_4$-biotinidase resistant biotin, c) conjugation with m-MeATE, d) charge modification using succinic anhydride, e) ^{211}At-labeling.

5.2.2 IN VITRO *ANALYSIS*

The degree of biotinylation and the number of free amino groups on the m-MeATE-B-PL_{suc} conjugate was determined using the 4'-hydroxyazobenzene-2-carboxylic acid (HABA) and 2,4,6-trinitrobenzene sulfonic acid (TNBSA) methods, respectively. The radiochemical purity (RCP) of the ^{211}At-labeled effector molecules was evaluated by methanol precipitation or instant thin-layer chromatography (ITLC), in addition to FPLC, and the avidin-binding ability was evaluated using avidin-linked agarose beads.

The efficiency of the developed pretargeting system was assessed in terms of cell binding using the same type of assay as for the labeled pretargeting molecule. Following a 2 h incubation of avidin-trastuzumab and cells in different dilutions, pretargeted cells were washed and resuspended in cell medium after which a small amount of effector molecule was added to the cell suspensions. After 1 h of incubation, the cells were washed once more and the B/T calculated following radioactivity measurements of the different dilutions.

In Paper II, the dissociation of cell bound Av-MX35 was assessed by incubating pretargeted cells in suspension at 37°C for up to 48 h. The cells were then washed and effector molecule added. After 1 h of incubation, cell binding was determined by calculating the B/T.

5.3 ANIMAL EXPERIMENTS

The studies described in Papers II–IV used nude mice (Balb/c *nu*/*nu*). All animal experiments were performed in accordance with protocols approved by the ethics committee of the University of Gothenburg.

5.3.1 PAPER II

In Paper II, *in vivo* distributions were performed in tumor-free animals (5–9 weeks of age) that were provided a biotin-deficient diet 5–7 d prior to the experiments. Biodistributions of i.p. injected ^{125}I-labeled Av-MX35 (40 kBq/25 µg) and ^{211}At-B-PL_{suc} (500 kBq/5 µg) were studied separately in groups of five mice per time point. Organs and tissues were harvested, weighed, and measured for radioactive content at 1, 3, 6, 10–11, and 24 h post injection (p.i). To study the effect of a blocking agent against unspecific uptake of free astatine, the ^{211}At-B-PL_{suc} distribution study was repeated, with the addition of two i.p. injections of sodium perchlorate prior to administration of the effector molecule. Supplementary distributions were performed to evaluate uptake in kidneys at early time points (15 min, 30 min, and 3 h p.i.) and to assess red bone marrow uptake (RBM; 1, 3, 6, 9, and 22 h p.i.). In addition, myelotoxicity was evaluated following administration of ^{211}At-B-PL_{suc} by measuring white blood cell (WBC) counts at 0, 5, and 14 d p.i.

To confirm specific tumor targeting, a small study was conducted using the α-camera technique developed by Bäck and Jacobsson [112], including four mice with i.p.

inoculated tumors. Two animals received PRIT using Av-MX35 and ^{211}At-B-PL$_{suc}$, and two received conventional RIT using ^{211}At-labeled MX35 F(ab')$_2$ fragments. The mice were sacrificed at 4 h p.i., at which point their spleens were removed and prepared for sectioning and α-camera imaging.

5.3.2 PAPER III

In Paper III, PRIT (Av-MX35 + ^{211}At-B-PL$_{suc}$, 1.0 or 1.5 MBq) was compared with conventional RIT (^{211}At-MX35 IgG, 0.9 MBq) for treatment of ovarian microtumors, and mice were inoculated i.p. with 1×10^7 NIH:OVCAR-3 cells in 0.2 mL cell medium. Tumors were allowed three weeks to establish, after which therapy (RIT or PRIT) was administered, with 20 animals per therapy group. The status of the mice was followed closely for the duration of the study, and individuals with signs of high tumor burden or poor general condition were euthanized. After eight weeks, all remaining animals were sacrificed and analyzed with regard to presence of ascites and tumors, and the tumor-free fraction (TFF) was calculated for each therapy group.

Suppression of WBC, platelets (PLT), and hemoglobin (HGB) was also studied in tumor-free mice after injection of ^{211}At-B-PL$_{suc}$ and ^{211}At-MX35.

5.3.3 PAPER IV

In Paper IV, systemic biodistributions were compared for PRIT and RIT in tumor bearing mice. Subcutaneous (s.c.) tumors were established by inoculating 1×10^7 NIH:OVCAR-3 cells via two s.c. injections in the scapula region. After 20–23 d, the xenografts measured 3–12 mm in diameter at which point the biodistributions were initiated. In the PRIT scheme, a dendrimeric CA containing 16 biotinylated *N*-acetyl-galactosamine residues and a single biotin moiety per molecule (NAGB; kindly provided by Dr. Oliver Press at the Fred Hutchinson Cancer Research Center, Seattle, WA, USA) was used for clearance of circulating SAv-MX35. A total of 20 mice were i.v. injected with 40 µg of SAv-MX35, followed by 10 µg of NAGB 12 h later. One hour after that, 1.3–1.5 MBq/1 µg of ^{211}At-B-PL$_{suc}$ was injected. Animals were then sacrificed and dissected at 0.5, 1, 3, 8, and 25 h p.i. (n = 4 per time point). In addition, three mice were injected with only ^{211}At-B-PL$_{suc}$ (i.e. without pretargeting) to separately assess blood clearance of the effector molecule. For comparison with conventional RIT, 15 mice were i.v. injected with 1.1–1.3 MBq/4 µg of ^{211}At-MX35, and subsequently sacrificed and dissected according to the protocol for the PRIT mice (n = 3 per time point).

6. DOSIMETRY

6.1 WHOLE-TISSUE DOSIMETRY

The definition of absorbed dose is the energy absorbed in a specific volume divided by the mass of the volume, i.e. the average energy density of a specific volume. Currently, the most commonly used methodology for estimating the absorbed dose from α-particles to a tumor or normal organ is whole-tissue dosimetry, assuming uniformly deposited α-particle energy throughout the volume of interest [67].

From the data obtained in the biodistribution studies (Papers II and IV), mean activity concentrations in the collected organs and tissues were calculated and compared to the amount of injected radionuclide, expressed as the percent injected activity per gram of tissue (%IA/g). This was done for all time points p.i., rendering a time-activity curve for each collected organ describing the pharmacokinetics of the administered substances. From this data, the mean absorbed dose D (Gy) was estimated using the formula

$$D = \frac{\tilde{A} \cdot \Delta \cdot \Phi}{m}$$

where $\tilde{A}$ is the cumulated activity (Bq·s), Δ is the mean energy released per decay (1.08×10^{-12} J $[\text{Bq}\cdot\text{s}]^{-1}$), Φ is the absorbed fraction of the α-particles (assumed to be 1), and m is the exposed mass (kg). This only includes contribution from α-particles; dose contribution from emission of electrons and photons is neglected. For each tissue, cumulated activity was calculated by integrating the time-activity curves. In Paper II, the absorbed dose to the thyroid was estimated from uptake in the throat, assuming that all activity in the throat was associated with the thyroid, using a standard weight for the thyroid of 3 mg. In Paper IV, the %IA/g in blood at the time of injection (0 h p.i.) was estimated at 67%, by assuming a blood volume of 1.5 mL (1.5 g) in mice.

The aim of PRIT is to deliver higher and more uniform absorbed doses to tumors than obtained using conventional RIT while sparing normal tissues. Different tissues exhibit different sensitivity to irradiation, and organisms are able to tolerate some loss of organ function before the induced toxicity becomes too severe. Hence, it is of crucial importance to identify organs whose loss of function limits the amount of radioactivity that can be administered by different therapy regimens. Knowing the dose-limiting organ for a certain treatment strategy, the maximum tolerable dose (MTD) can be determined, which corresponds to the maximum tolerable activity (MTA), i.e. the amount of the radiolabeled substance that can be injected using that particular strategy. The possible efficacy of the treatment is then determined by the absorbed dose to tumor that can be delivered by injection of the MTA. The utility of a therapeutic strategy is determined by the relationship between the absorbed dose to tumor and the dose to critical normal organs; a relation that is sometimes called the “therapeutic window”. The span of the therapeutic window can be assessed by calculating the tumor-to-normal tissue dose ratio (TNTDR). In Paper IV, TNTDRs were calculated for systemic PRIT using

SAv-MX35 and ^{211}At-B-PL$_{suc}$ and compared with the corresponding ratios for conventional RIT using ^{211}At-MX35 IgGs. Historical *in vivo* data for ^{211}At-labeled F(ab')$_2$ fragments was also included in the comparison.

6.2 Cell-Level Dosimetry

In Paper III, cell-level dosimetry was used to compare the dose contributions from specific irradiation in the conducted i.p. therapies using conventional RIT (^{211}At-MX35 IgG, 0.9 MBq) and PRIT (^{211}At-B-PL$_{suc}$, 1.0 or 1.5 MBq). Mean absorbed doses were analytically estimated for isolated cells and cells located at the borders of metastases, using a cell-level dosimetry code developed by Chouin et al. [113].

In short, the number of decays (n) that occurred on the surface of a single cell was estimated for each therapy regimen using the α-camera. A cell and its nucleus were then modeled as two concentric spheres filled with water, and the probability (P) of one α-particle emitted at the cell surface crossing the nucleus calculated via a simple geometrical relation. The amount of α-particles that would travel through the nucleus could then be estimated by multiplying n and P. However, α-particles will traverse different parts of a spherical nucleus: some tracks will cross through the middle and some will cross closer to the edge. Depending on the length of the tracks, various amounts of energy will therefore be deposited. The different outcomes were computed using the small-scale dosimetry algorithm of Chouin et al., resulting in a mean value of absorbed dose per α-particle track ($\langle z_1 \rangle$). The algorithm assumes that the α-particles travel through the nucleus following a straight line, depositing energy according to the continuous slowing-down approximation. The mean absorbed dose per cell (D) was thereafter calculated by multiplying $\langle z_1 \rangle$, n, and P.

7. RESULTS

7.1 *IN VITRO* PRETARGETING MODEL (PAPER I)

Conjugation of avidin to trastuzumab resulted in an overall yield of 2–11% after purification. Results were limited by the fact that a large portion of the mAb remained unbound to avidin, and a small fraction of unwanted di- and polymeric compounds were formed. Even after purification, approximately 17% of the solution consisted of larger Av-mAb complexes. The MW of the avidin-trastuzumab monomers was estimated using SDS-PAGE to be approximately 220 kDa, which was expected considering the individual MWs of the conjugated proteins. The ^{211}At-labeled pretargeting molecule bound well (86–95%) to immobilized iminobiotin and the maximum B/T was 64% after incubation with SKOV-3 cells (nonspecific binding <10%). This verified that the avidity for biotin was good and that the targeting ability of the mAb was more or less intact after conjugation.

^{211}At-labeling of biotinylated poly-L-lysine was performed with 26–77% radiochemical yield and a resulting RCP of 92–97%. The avidin-binding ability was excellent, with 91–93% of the added radioactivity bound to the beads after 1 h incubation. Despite previous concerns of harming the biotin moiety with oxidative agents [105], the direct one-step astatination procedure proved successful for this poly-L-lysine based effector molecule; a notable benefit for enabling delivery of therapeutic absorbed doses, considering the short half-life of ^{211}At. Succinylation led to increased MW of the effector molecule by approximately 70% compared with the MW of the initial poly-L-lysine molecule. Naturally, an effector molecule of that size (220 kDa) will hardly be useful in therapeutic settings, but the methods developed for its synthesis and labeling can be employed in the production of smaller, peptide-based molecules for future *in vivo* studies.

The full pretargeting assay resulted in a maximum B/T of approximately 75% after 1 h incubation of ^{211}At-B-PL$_{suc}$ and Av-trastuzumab-pretargeted SKOV-3 cells (nonspecific binding <1%). Figure 5 shows the binding curve. Although synthesis and purification of the pretargeting molecule should be further improved, proof-of-concept was shown for this *in vivo* pretargeting system. The efficient and specific binding of the ^{211}At-labeled effector molecule to pretargeted cells encouraged further development and application of the system *in vivo*.

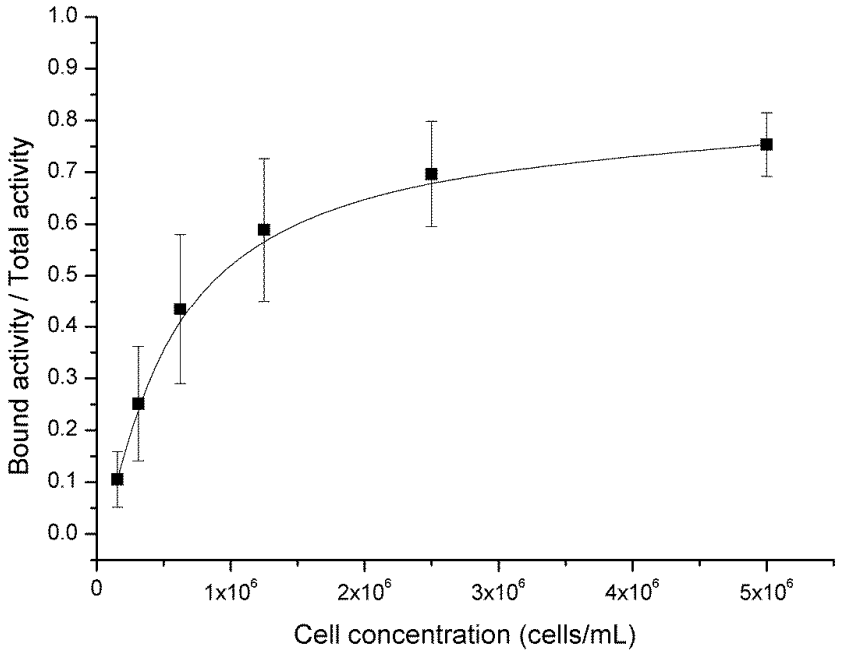

FIGURE 5. Binding of ^{211}At-B-PL$_{suc}$ to Av-trastuzumab-pretargeted SKOV-3 cells (mean ± SD, *n* = 5).

7.2 I.P. DISTRIBUTIONS OF ^{125}I-AV-MX35 AND ^{211}AT-B-PL$_{SUC}$ (PAPER II)

The synthesis and astatination of the small, biotinidase-resistant effector molecule was convenient and straightforward. Efficient ^{211}At-labeling of the m-MeATE-B-PL$_{suc}$ conjugate was achieved, with a radiochemical yield and RCP of approximately 85% and 99%, respectively. The effector molecules contained 1.5 biotin moieties per peptide on average, as determined by the HABA method. TNBSA analysis showed that the succinylation of the poly-L-lysine was basically complete, as no free amino groups were detected on the m-MeATE-B-PL$_{suc}$ conjugate. Hence, the MW of the final ^{211}At-B-PL$_{suc}$ effector molecule was estimated to be approximately 7700 kDa, a doubling compared to the weight of the initial poly-L-lysine peptide.

The stability over time of the Av-MX35–NIH:OVCAR-3 bond was satisfactory: after incubation of the pretargeted cells for 6 h at 37°C, the bound fraction of ^{211}At-B-PL$_{suc}$ decreased to 64% of the B/T value after 1 h incubation. After that, the decrease was more modest with 62% and 57% of the 1 h-B/T values at 24 and 48 h, respectively. This indicated that adequate tumor targeting can be achieved in complete PRIT studies administering the effector molecule 24 h after the pretargeting molecule, as a sufficient amount of Av-MX35 remained on the cell surface for at least 48 h *in vitro*.

The clearance of ^{125}I-labeled pretargeting molecule produced the expected results: glycosylation of avidin promoted rapid transportation of the ^{125}I-Av-MX35 conjugate to the liver. At 24 h p.i., the %IA/g was low in all collected tissues and organs of interest. A preliminary experiment was also performed, in which ^{211}At-B-PL$_{suc}$ was injected at various times (1, 3, 6, 24, and 48 h) after administration of Av-MX35. The resulting uptake in liver and kidneys were thereafter compared, indicating initial binding of the effector molecule to circulating pretargeting molecules. At 24 h p.i., the activity distribution correlated with that of independently administered ^{211}At-B-PL$_{suc}$, supporting the choice of a 24 h-period for tumor localization and clearance between the two administrations.

Figure 6 illustrates the distribution of ^{211}At-B-PL$_{suc}$. In panel A no blocking agent was administered, and elevated ^{211}At levels were recorded in tissues that are known to accumulate free astatine, such as the throat, salivary glands, lungs, stomach, and spleen. However, the effect of injecting sodium perchlorate before administration of the effector molecule was considerable, as shown in panel B. The most significant reduction was observed in the throat, where uptake decreased by almost nine-fold. Stomach and salivary glands also showed lower %IA/g; their uptake was reduced by approximately five- and three-fold, respectively. Lungs and spleen showed more modest reductions. Kidney uptake confirmed that the main route of clearance for the labeled peptide was via renal excretion. Because of the rapid clearance, an additional study including two earlier time points, 15 and 30 min p.i., was conducted to enable adequate dosimetry for the kidneys. Figure 7 shows the combined results, revealing that renal uptake peaked around 1 h p.i. with approximately 19%IA/g, after which a rapid decrease occurred to 2%IA/g at 6 h p.i.

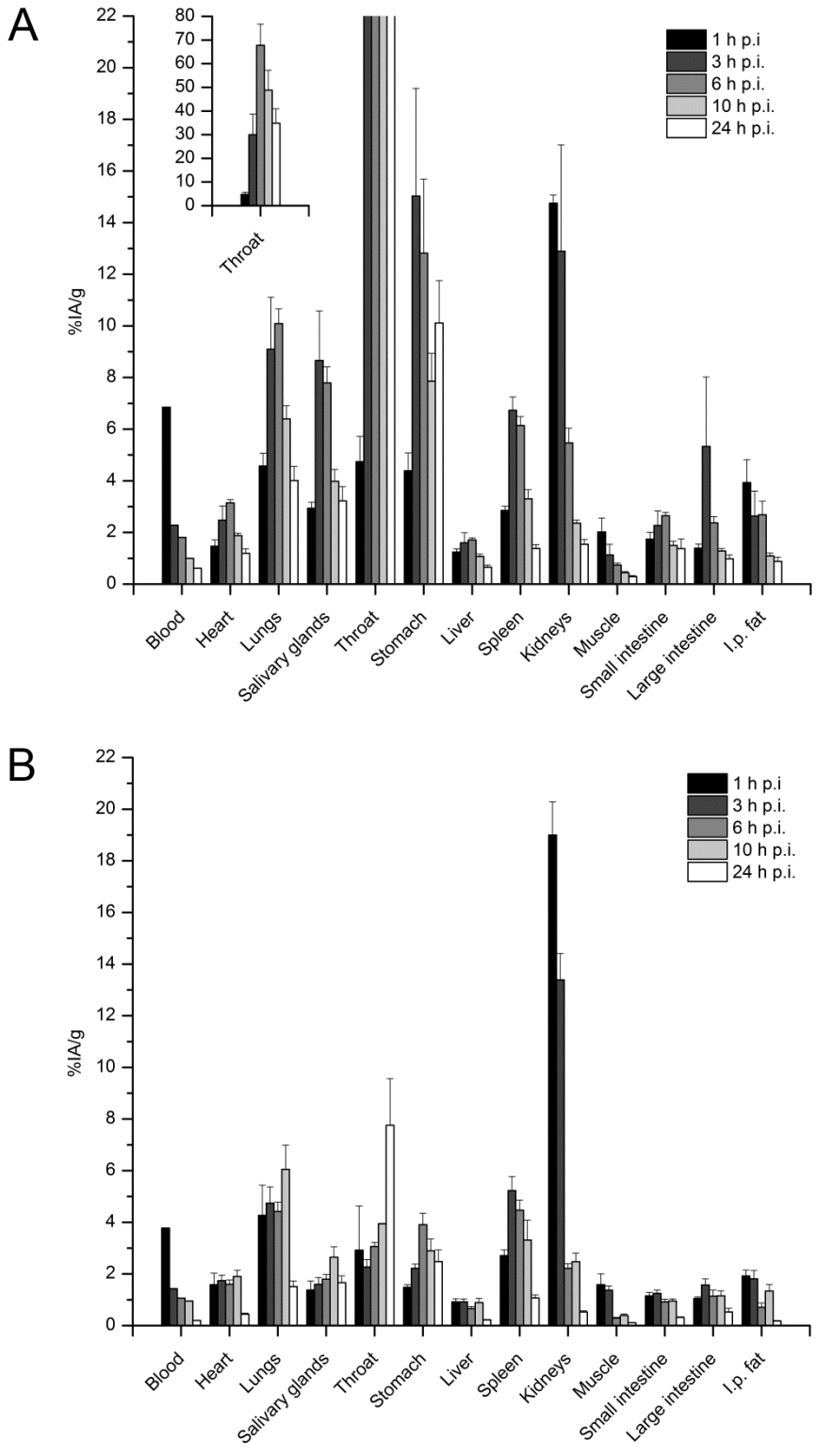

FIGURE 6. Distribution of ^{211}At-B-PL$_{suc}$ in tumor-free mice 1–24 h after i.p. administration (n = 5 per time point). Uptake is expressed as mean ± SEM, except in blood for which the median value is shown. A) No administration of blocking agent. B) Animals were given sodium perchlorate at 24 h and 1 h before injection of ^{211}At-B-PL$_{suc}$ to block uptake of free ^{211}At.

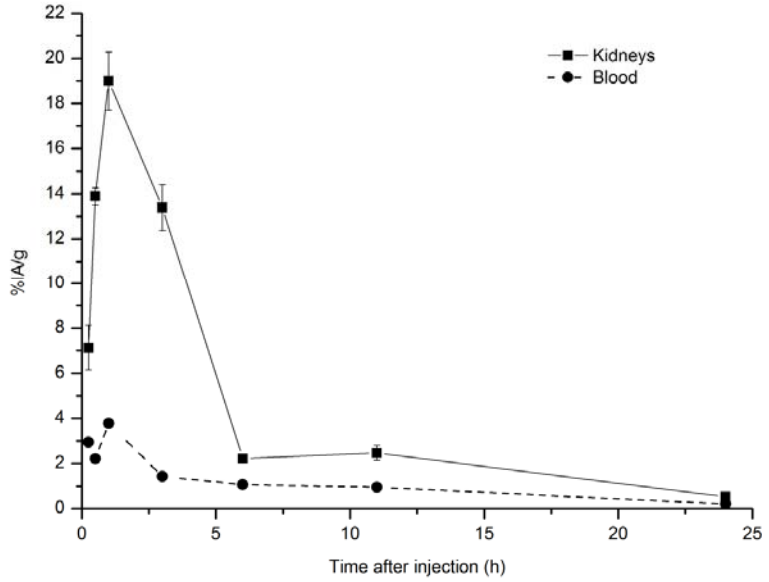

FIGURE 7. Blood clearance (median value) and uptake of ^{211}At in kidneys (mean ± SEM) after i.p. injection of ^{211}At-B-PL$_{suc}$ in tumor-free mice in two separate experiments (*n* = 5 per time point). Data for 1 to 24 h is combined with uptake at 15 and 30 min from another study. Animals were given sodium perchlorate at 24 h and 1 h before injection of ^{211}At-B-PL$_{suc}$ to block uptake of free ^{211}At.

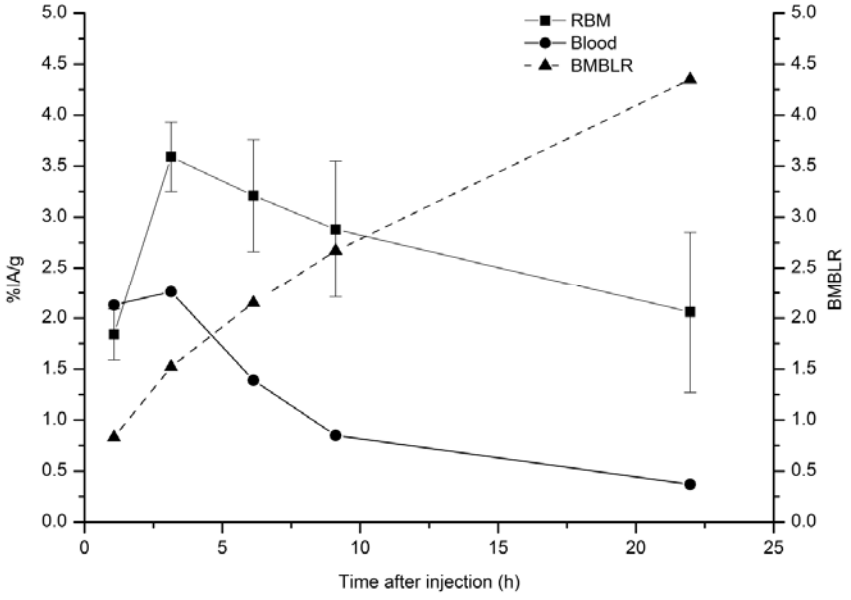

FIGURE 8. Blood clearance (median value) and uptake in RBM (mean ± SEM) of ^{211}At after i.p. injection of ^{211}At-B-PL$_{suc}$ in tumor-free mice, combined from two separate experiments (*n* = 4 per time point). The BMBLR was calculated by dividing the %IA/g in RBM for each time point with the corresponding value in blood. Animals were given sodium perchlorate at 24 h and 1 h before injection of ^{211}At-B-PL$_{suc}$ to block uptake of free ^{211}At.

Figure 8 depicts the blood clearance and uptake in RBM together with the bone marrow-to-blood ratio (BMBLR), which was calculated for each time point by dividing the %IA/g in RBM with the corresponding value in blood. An unexpected finding was the apparent accumulation of ^{211}At in the RBM, seemingly uncorrelated to the activity concentration in blood, shown by the steady increase in BMBLR for at least 22 h p.i.

Mean absorbed doses were estimated for all collected organs and tissues, expressed in Gy per i.p. injected MBq of ^{211}At-B-PL$_{suc}$. Figures of interest were 1.9 Gy/MBq for lungs, 1.2 Gy/MBq for spleen, 2.3 Gy/MBq for kidneys, 1.8 Gy/MBq for throat (18.2 Gy/MBq for thyroid), and 0.9 Gy/MBq for RBM. Renal toxicity is generally considered to be a potential dose-limiting effect in RIT, but Bäck et al. found that a mean absorbed dose to the kidneys of approximately 10 Gy using ^{211}At-labeled MX35 F(ab')$_2$ fragments is tolerable with regard to glomerular filtration rate (GFR) [114]. It is therefore unlikely that renal uptake will be crucial in this pretargeting model. Uptake in the lungs and spleen showed that the sodium perchlorate blocking has room for improvement. The administration scheme used in this study was proposed by Larsen et al., who also suggested the use of multiple substances for more efficient minimization of normal tissue uptake of free ^{211}At [115]. The estimated absorbed dose to the thyroid stood out from those of other organs, but it should be noted that it was based on several approximations that greatly influenced the outcome and should thus not be given too much significance. Of greater interest was the absorbed dose to RBM, which was higher than anticipated based on the low activity concentration in blood; this was due to the unforeseen accumulation revealed by the BMBLR. The underlying mechanisms for this accumulation are unknown, but it highlights the importance of measuring the actual uptake in bone marrow and not just estimating its absorbed dose from blood data. No severe toxicity was observed from the activities administered in the myelotoxicity study, which corresponded to absorbed doses of 0.0, 0.2, 0.5, 0.7, and 0.9 Gy, showing that at least 1.0 MBq of ^{211}At-B-PL$_{suc}$ can be safely administered. Previous studies of conventional i.p. RIT with ^{211}At-labeled mAbs demonstrated that 1.0 MBq is a level of activity that can be expected to be curative [92].

Figure 9 shows images attained using the α-camera. Specific uptake in tumor cluster areas compared with uptake in the spleen was clearly seen for both PRIT (panel A) and conventional RIT (panel B). The overlay images in panels C and D confirmed that the high activity areas outside the spleen corresponded to clusters of tumor cells visible on the H&E sections. From this it can be deduced that specific targeting was reached for the pretargeting strategy, at levels that corresponded to those achieved using conventional RIT.

Data gained from these biodistribution studies and *in vitro* experiments were used to establish a suitable scheme for dosing and timing in i.p. therapy studies of ovarian cancer in mice. We concluded that good tumor targeting and acceptable toxicity could be reached following i.p. injection of 1.0 MBq of ^{211}At-B-PL$_{suc}$ 24 h after injection of Av-MX35.

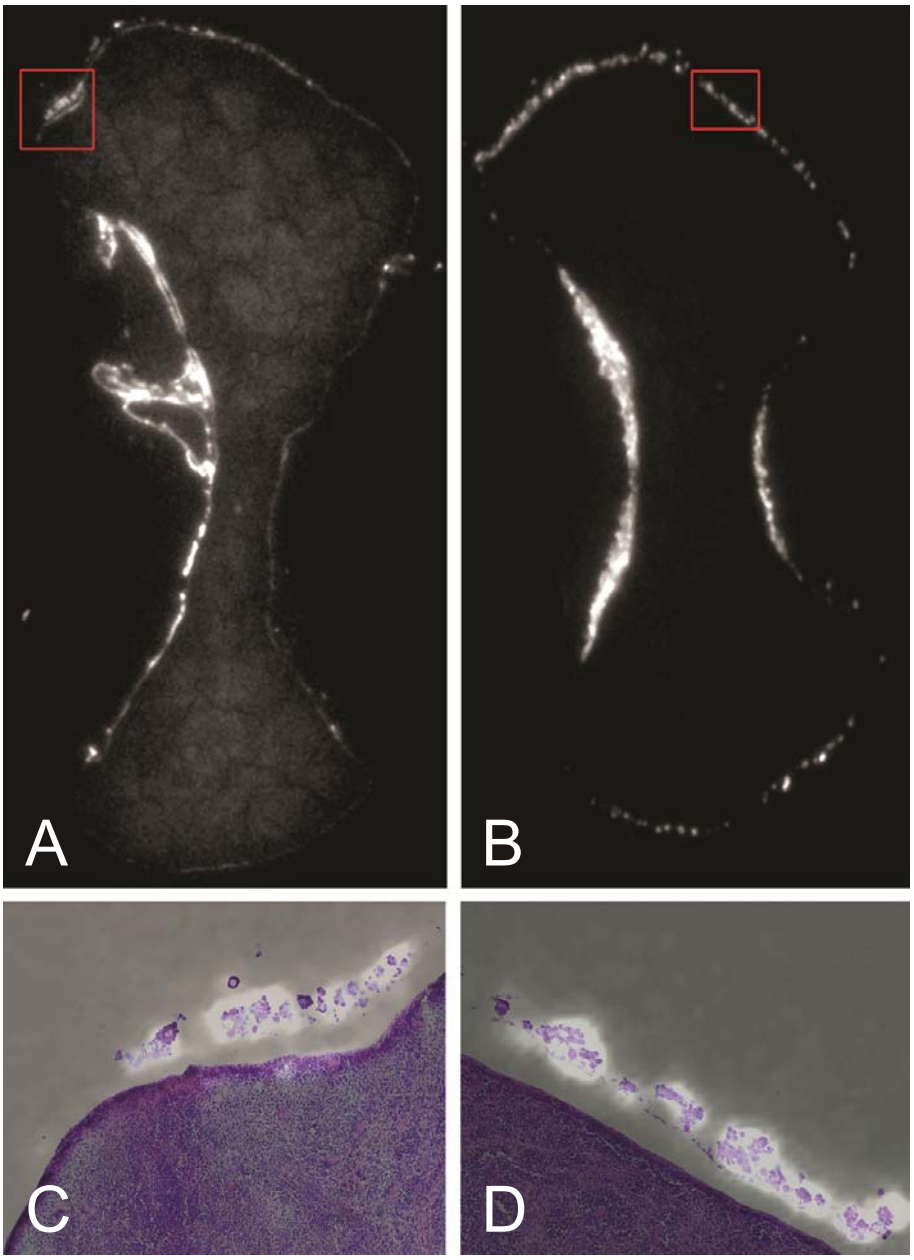

FIGURE 9. α-camera images showing the distribution of ^{211}At in cryosectioned spleens after i.p. administration of Av-MX35 + ^{211}At-B-PL$_{suc}$ (A) and ^{211}At-MX35 F(ab')$_2$ (B) to tumor-carrying mice. Marked regions of interest (in red) show high intensity areas that are overlaid with the corresponding areas in H&E-stained sections shown in (C) and (D). Areas displaying high activity correspond well with the location of tumor cells, confirming specific uptake of ^{211}At for both targeting regimens.

7.3 COMPARISON OF ^{211}AT-PRIT AND ^{211}AT-RIT (PAPER III)

The ^{211}At-labeling of m-MeATE-B-PL_{suc} and MX35 IgG was successfully performed with radiochemical yields of 66% and 76%, respectively, and RCP of >99% for both astatinated products. At the time of labeling, specific activity was 2.8 MBq/μg for ^{211}At-B-PL_{suc} and 0.3 MBq/μg for ^{211}At-MX35. Both systems produced equally good *in vitro* binding to NIH:OVCAR-3 cells, with 85% maximum B/T. The biotinylation degree of the effector molecule was higher than in Paper II, with approximately three biotin moieties per poly-L-lysine molecule.

Figure 10 shows results from the hematology study in tumor-free mice. A significant ($P<0.05$) reduction in WBC and PLT was seen 5 d p.i. for all irradiated groups compared to the control group. The highest mean WBC suppression (93%) was recorded for the 1.5-MBq ^{211}At-B-PL_{suc} group at 5 d p.i., but all animals in that study group recovered their baseline WBC count at 21 d p.i. Corresponding reductions in WBC were 78% for the 1.0-MBq ^{211}At-B-PL_{suc} group and 89% for the 0.9-MBq ^{211}At-MX35 group. No effect on HGB was observed in any group.

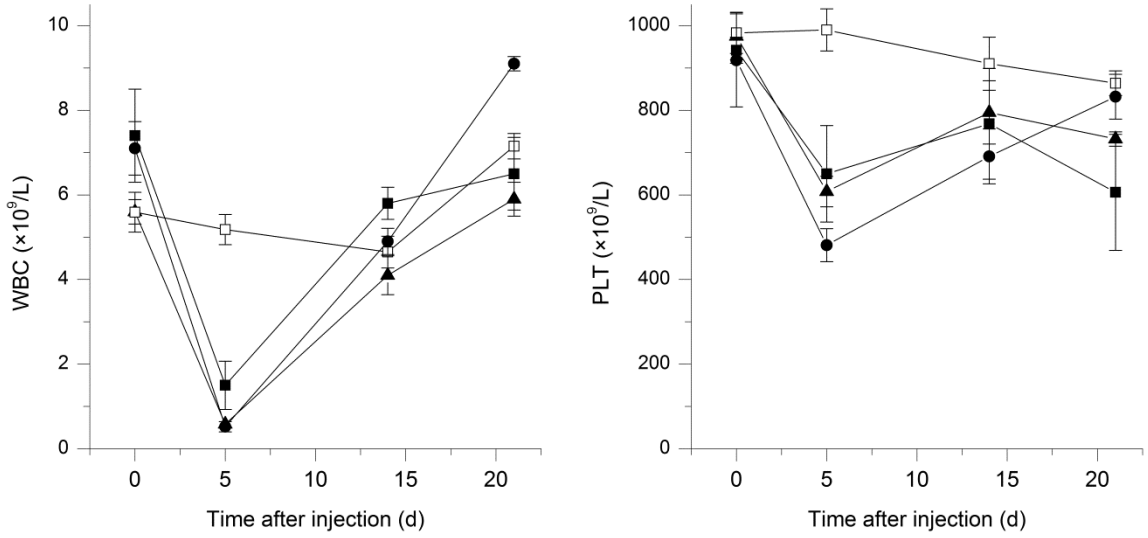

FIGURE 10. White blood cell (WBC) and platelet (PLT) counts (means ± SEM) as a function of time after i.p. injections of ^{211}At-B-PL_{suc} (1.0 MBq, ■; 1.5 MBq, ●; *n*=5), ^{211}At-MX35 (0.9 MBq, ▲; *n*=5), or PBS (□; *n*=10). A significant reduction in WBC and PLT counts ($P<0.05$) was recorded at day 5 p.i. for the irradiated groups compared with the non-irradiated control group.

Among the inoculated mice, ten were dedicated for sacrifice at the time of therapy to assess tumor status. Seven of these mice displayed ascites, predicting poor therapy results as previous studies of this particular tumor model showed that initial tumor status strongly influences therapeutic outcome and that mice with ascites are more difficult to cure using ^{211}At-RIT [89, 93]. Table 1 summarizes the results for all groups

eight weeks after therapy in terms of presence of ascites, tumor growth, and TFF. Tumor growth was assessed by ocular inspection at the time of dissection and by light microscopy examination of H&E-stained biopsy samples from the peritoneum, i.p. fat, diaphragm, and small intestine. All untreated animals developed ascites and tumors, and the TFF for the different therapy groups were 0.35 (PRIT 1.0 MBq), 0.45 (PRIT 1.5 MBq), and 0.45 (RIT). Tumors identified microscopically were also differentiated into two groups based on size, with one group consisting of tumors ranging from single cells to cell clusters of approximately 1 mm in diameter and the second group including all larger tumors. By doing this, a more nuanced representation of the therapy results emerged. Although the TFFs were equal for the 1.5-MBq PRIT group and the RIT group, only 3/11 (27%) animals with confirmed tumors displayed tumor sizes >1 mm in the PRIT group versus 8/11 (73%) in the RIT group. Figure 11 illustrates the result of this differentiation. Another major difference was the presence of ascites at the end of the study: in the RIT group, 40% of mice had ascites, but in the 1.5-MBq PRIT group no ascites was found eight weeks after therapy. This indicated that high-activity PRIT may have been more efficient than conventional RIT. Better penetration and thereby more uniform distribution of radioactivity for PRIT could explain the observed differences, but other important factors were the amount of ^{211}At-labeled molecules administered in the different regimens and the resulting specific irradiation of tumor cells. The incidence of ascites in the ten animals sacrificed at the start of therapy indicated that the disease stage was more advanced than anticipated when designing the study. From estimations of the number of available antigens for mice with ascites, it could be concluded that the injected amounts of radiolabeled molecules were insufficient for both PRIT and RIT. Using small-scale dosimetry, mean absorbed doses from specific irradiation were calculated for isolated tumor cells, resulting in <10 Gy for the RIT group and the 1.0-MBq PRIT group. For the 1.5-MBq PRIT group the mean absorbed dose was approximately 15 Gy. The perceived difference in therapeutic outcome could thus pertain to the difference in administered activity for the various therapy groups.

The amount of activity that can be injected is restricted by irradiation of normal tissues, and Elgqvist et al. showed that the MTA for ^{211}At-labeled MX35 IgG is approximately 1.2 MBq [116]. In Paper II, we concluded that 1.0 MBq of i.p. administered ^{211}At-B-PL$_{suc}$ was a safe activity, but data from additional studies indicated that the MTA was somewhat higher. We therefore included the 1.5-MBq PRIT group in this therapy study, and the hematology data showed that our supposition was correct. In future therapy studies, comparisons of PRIT and RIT should be performed with activities equal to the MTA for each strategy to evaluate if a therapeutic gain can be achieved using PRIT.

In the current setting, we can conclude that the PRIT strategy was at least as good as RIT for eradicating microscopic ovarian tumors in mice. Despite an advanced disease stage, the resulting TFF shows proof-of-concept for the pretargeting system *in vivo*, and encourages further studies.

TABLE 1.
Study groups and number of mice with tumors and ascites

Group	*n*	Treatment	Activity (MBq)	Ascites	Macroscopic tumors found at dissection	Tumors found by microscopy	TFF
PRIT 1	20	^{211}At-B-PL$_{suc}$ + Avidin-MX35	0.955–1.004	3/20	3/20	13/20	0.35
PRIT 2	20	^{211}At-B-PL$_{suc}$ + Avidin-MX35	1.480–1.542	0/20	1/20	11/20	0.45
RIT	20	^{211}At-MX35	0.784–0.878	8/20	3/20	11/20	0.45
Control	19*	PBS	—	19/19	18/19	19/19	0

*One mouse without signs of tumor growth or ascites was sacrificed prematurely due to deterioration

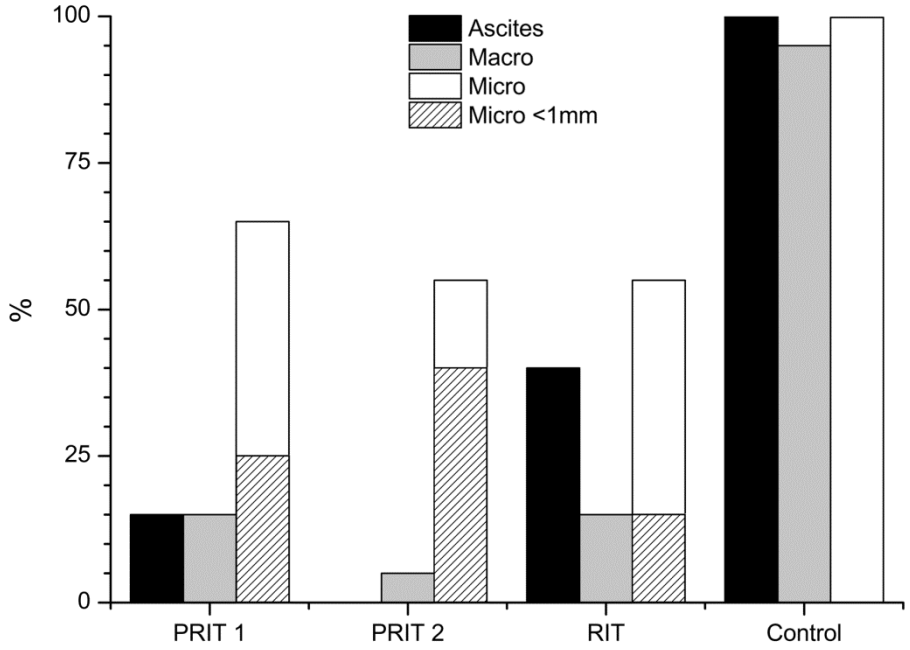

FIGURE 11. Comparison of therapy results. Ascites = animals with ascites found at dissection; Macro = animals with macroscopic tumors found at dissection; Micro = animals with tumors found by microscopy, total; Micro <1 mm = animals with tumors found by microscopy, only <1 mm.

7.4 Systemic Distribution of ^{211}At-B-PL$_{suc}$ (Paper IV)

Astatination of m-MeATE-B-PL$_{suc}$ and MX35 IgG resulted in specific activities of 1.5 MBq/µg for ^{211}At-B-PL$_{suc}$ (RCP 99%) and 0.3 MBq/µg for ^{211}At-MX35 (RCP 98%) at the time of injection. Excellent avidin-binding ability was seen for the effector molecule, with 97% of the added activity bound to avidin agarose beads after 1 h incubation. In NIH:OVCAR-3 cell assays, the maximum B/T was 73% for ^{211}At-MX35 but only 16% for ^{211}At-B-PL$_{suc}$. The latter was most likely due to partial deterioration and aggregation of the SAv-MX35 pretargeting molecule.

Figure 12 shows the biodistributions after i.v. injection of SAv-MX35 + NAGB + ^{211}At-B-PL$_{suc}$ and ^{211}At-MX35 IgG. The small effector molecule displayed rapid clearance: only 8%IA/g remained in blood at 30 min p.i. and at 25.5 h p.i. the activity concentration was down to 1%IA/g. Tumor uptake was exceptionally fast, with 7%IA/g already at 30 min p.i. and a peak of 11%IA/g at 1 h p.i. The tumor associated activity then decreased to approximately 2%IA/g at 25 h p.i. For RIT, almost reverse circumstances were observed: the activity concentration in blood was approximately constant at around 30%IA/g from 1 to 8 h p.i, decreasing to 16%IA/g at 25 h p.i. Compared with PRIT, tumor uptake was slow but increased steadily reaching 15%IA/g at 25 h p.i. In agreement with the i.p. results in Paper II, the effector molecule in the PRIT regimen accumulated in the RBM. Elevated levels of ^{211}At in RBM were also seen using the RIT strategy, but they were most likely the result of the long retention of ^{211}At-MX35 in blood. This was verified by calculation of the BMBLR, which for RIT was fairly constant at approximately 0.3, a ratio that generally corresponds to blood borne radioactivity. For PRIT, on the other hand, the BMBLR increased throughout the observation time indicating active accumulation. Figure 13 shows BMBLR plotted against time after injection.

Presence of free ^{211}At was indicated by elevated levels of radioactivity in the lungs and spleen for both treatment strategies. The uptake in other astatine-accumulating tissues, such as the throat, salivary glands, and stomach, was less pronounced because of efficient blocking by sodium perchlorate. For PRIT, free ^{211}At was released through rapid renal excretion, as indicated by the initially high but rapidly decreasing kidney uptake.

The effect of the NAGB CA was investigated through comparison of ^{211}At-B-PL$_{suc}$ clearance after administration according to the PRIT strategy or separately, i.e. without pretargeting. Figure 14 shows results from blood sampling. The presence of a small amount of retained SAv-MX35 conjugate was indicated by slower clearance using the PRIT strategy, showing that there may be room for some optimization of the injection scheme.

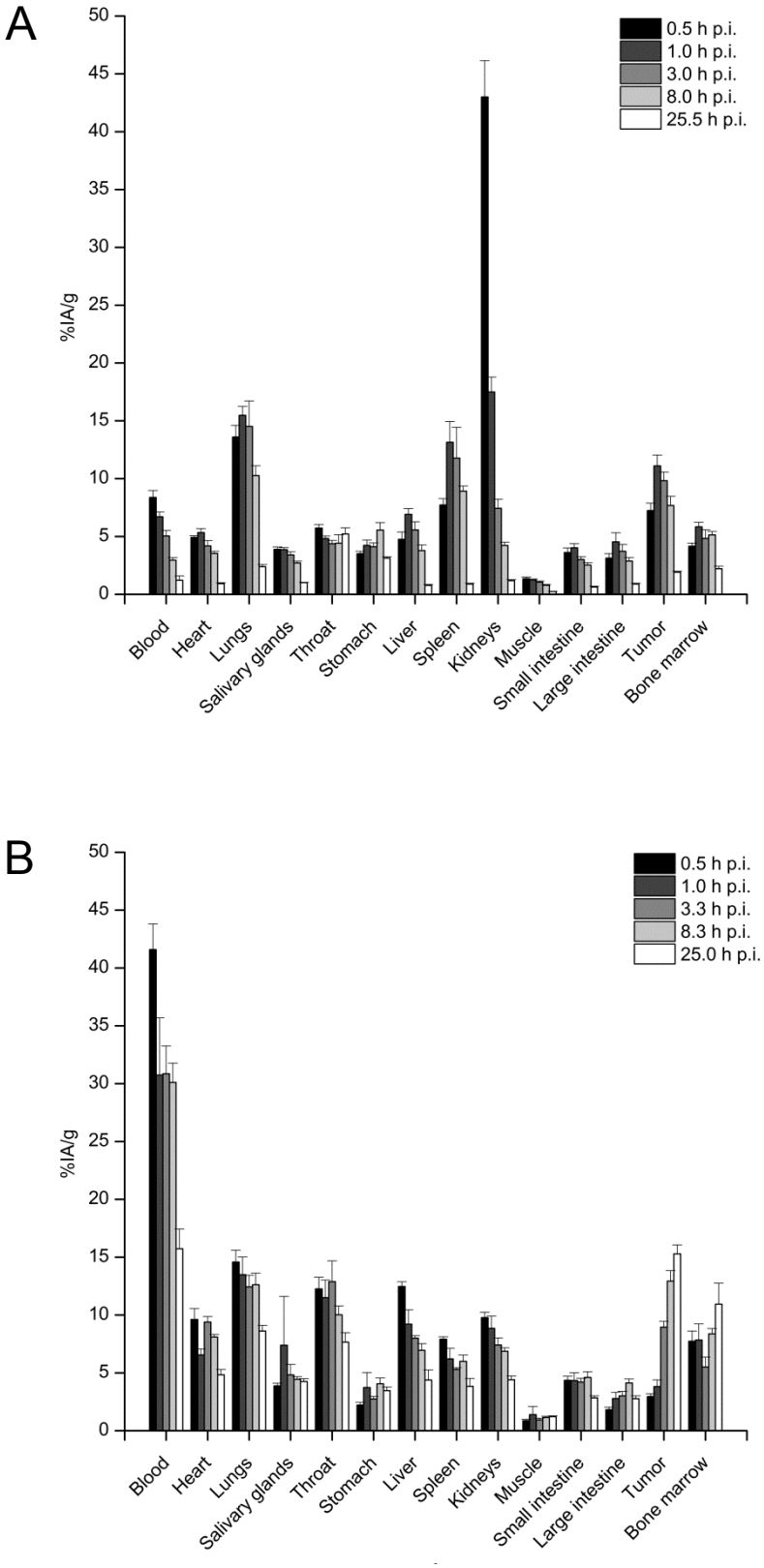

FIGURE 12. Biodistributions showing the uptake (mean ± SEM) of ^{211}At after systemic PRIT or RIT. Animals were given sodium perchlorate at 24 h and 1 h before i.v. injections of labeled substances to block uptake of free ^{211}At. A) PRIT, SAv-MX35 + NAGB + ^{211}At-B-PL$_{suc}$ (*n* = 4 per time point). B) RIT, ^{211}At-MX35 IgG (*n* = 3 per time point).

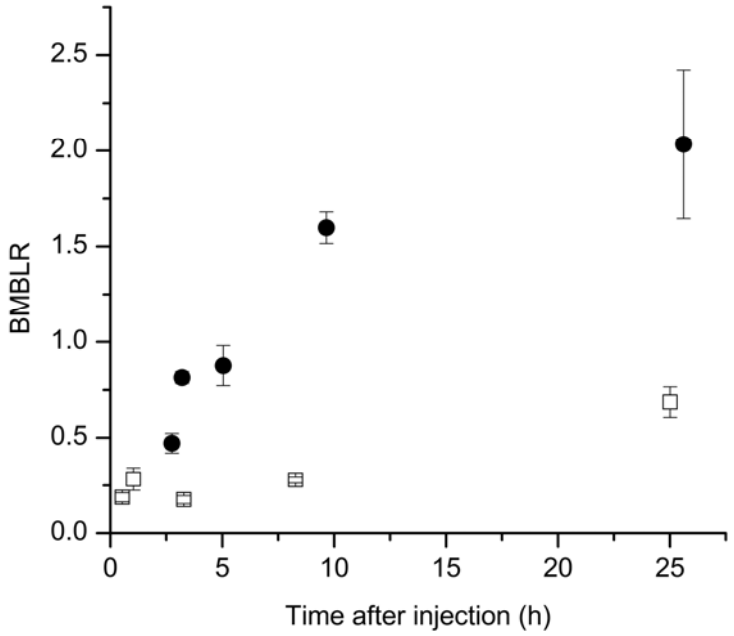

FIGURE 13. BMBLR (mean ± SEM) for PRIT (●; *n* = 4 except for 25 h p.i. where *n* = 3) and RIT (□; *n* = 3) at different times after i.v. injection of ^{211}At-B-PL$_{suc}$ or ^{211}At-MX35 in mice with subcutaneous tumors. The BMBLR was calculated as the %IA/g in RBM divided by the corresponding value in blood for each time point.

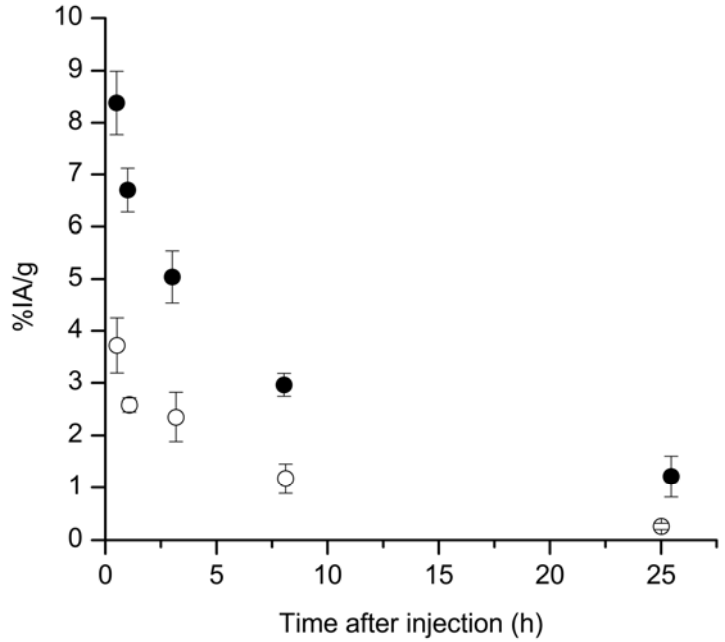

FIGURE 14. Activity concentration in blood expressed as %IA/g (mean ± SEM) for i.v. injected ^{211}At-B-PL$_{suc}$ either without pretargeting (○; *n* = 3) or after administration of SAv-MX35 and NAGB according to the full PRIT scheme (●; *n* = 4 except for 25 h p.i. where *n* = 3).

Table 2 contains the estimated mean absorbed doses expressed in Gy per MBq after i.v. administration of ^{211}At-B-PL$_{suc}$ and ^{211}At-MX35 IgG. For comparison, absorbed doses for ^{211}At-MX35 F(ab')$_2$ fragments were calculated from biodistribution data previously reported by Bäck et al. [117] and included in the table. It should be noted that the mice in the study by Bäck et al. received no blocking agent. For the PRIT strategy, absorbed doses of special interest were 4.6 Gy/MBq for lungs, 1.9 Gy/MBq for RBM, and 3.2 Gy/MBq for tumor. Conventional RIT strategies resulted in absorbed doses to tumors of just over 4 Gy/MBq. Although the absorbed dose to blood was markedly higher for IgG-RIT, the absorbed dose to RBM was roughly equal for both RIT strategies, and somewhat higher than that of PRIT. In Table 3 the resulting TNTDRs are shown for the three regimens. Only minor differences between PRIT and RIT were seen for RBM, lungs, and kidneys, organs and tissues that may be dose-limiting in this systemic setting.

The exceptionally high uptake of MX35-targeted radioactivity in subcutaneous tumors previously observed by Bäck et al. [117] was affirmed by these distributions, emphasizing the great potential for targeted therapy using this antibody. Moreover, results indicated that the absorbed dose to tumor may be increased substantially compared to conventional RIT using pretargeting, because of much faster tumor accretion of radiolabeled molecules. An apparent possibility of increasing the absorbed dose to tumor delivered by the PRIT strategy lies in the decreasing ^{211}At-localization observed in tumors over time. It seems as though the pretargeting molecule was released too quickly from the antigen sites, suggesting that the timing of the administrations could also be optimized in this respect. However, it is likely that the suspected issues with the SAv-MX35 conjugate indicated by the *in vitro* cell-binding assay also affected the *in vivo* behavior, underlining the significance of improvements in synthesis of the pretargeting molecule.

Considering the short half-life of ^{211}At, the rapid tumor uptake following pretargeting is very promising from a therapeutic point of view. With a more robust SAv-MX35 conjugate and optimization of the administration scheme, a broadening of the therapeutic window compared with conventional RIT seems highly realizable.

TABLE 2.

Mean absorbed doses after i.v. administration of ^{211}At-labeled substances in mice carrying s.c. tumors. PRIT = ^{211}At-B-PL_{suc} + NAGB + SAv-MX35 (*n* = 4) and RIT/IgG = ^{211}At-MX35 IgG (*n* = 3). Mean absorbed doses for RIT/F(ab')$_2$ were calculated from historical distribution data for ^{211}At-MX35 F(ab')$_2$ (*n* = 3) reported by Bäck et al. [117]. Mice in the PRIT and RIT/IgG experiments were treated with sodium perchlorate before injection of ^{211}At-labeled substances, but no blocking was used in the RIT/F(ab')$_2$ study.

	Absorbed dose (Gy/MBq)		
Organ	PRIT	RIT/IgG	RIT/F(ab')$_2$
Blood	2.3	12.4	5.7
Heart	1.5	3.2	2.0
Lungs	4.6	4.9	3.4
Salivary glands	1.2	1.9	2.8
Throat	1.8	4.3	10.9
Stomach	1.9	1.4	2.9
Liver	1.8	3.0	1.2
Spleen	3.8	2.3	1.5
Kidneys	3.2	2.8	4.0
Muscle	0.4	0.4	0.4
Small intestine	1.1	1.7	1.2
Large intestine	1.3	1.4	0.8
RBM[a]	1.9	3.0	3.2[b]
Tumor	3.2	4.1	4.2

[a]RBM = Red bone marrow

[b]Calculated from blood data using a BMBLR of 0.56

TABLE 3.

Tumor-to-normal tissue dose ratios (TNTDR) after i.v. administration of ^{211}At-labeled substances in mice carrying s.c. tumors. PRIT = ^{211}At-B-PL$_{suc}$ + NAGB + SAv-MX35 (*n* = 4) and RIT/IgG = ^{211}At-MX35 IgG (*n* = 3). TNTDR was calculated for the different regimens as the ratio between absorbed doses to tumors and corresponding normal tissue doses. Values for RIT/F(ab')$_2$ were calculated from historical data reported by Bäck et al. [117]. Mice in the PRIT and RIT/IgG regimens were treated with sodium perchlorate before injection of ^{211}At-labeled substances, but in the RIT/F(ab')$_2$ study no blocking was used.

	TNTDR		
Organ	PRIT	RIT/IgG	RIT/F(ab')$_2$
Blood	1.4	0.3	0.7
Heart	2.2	1.3	2.1
Lungs	0.7	0.8	1.2
Salivary glands	2.8	2.2	1.5
Throat	1.8	1.0	0.4
Stomach	1.7	2.9	1.5
Liver	1.9	1.4	3.5
Spleen	0.9	1.8	2.8
Kidneys	1.0	1.5	1.1
Muscle	9.0	9.3	9.6
Small intestine	3.0	2.4	3.6
Large intestine	2.6	3.0	5.4
RBM[a]	1.7	1.4	1.3[b]
Tumor	1.0	1.0	1.0

[a]RBM = Red bone marrow

[b]Calculated from blood data using a BMBLR of 0.56

8. Discussion and Conclusions

8.1 General

Malignant cells can detach and disseminate via the blood circulation or the lymphatic system, enabling metastatic spread throughout the body. In order to effectively reach all tumor cells during treatment, an efficient RIT modality should enable targeting molecules to transport along the same routes, but current techniques are in most cases limited by side effects caused by the narrow therapeutic windows. Radiation-induced cell death occurs primarily as cells attempt to divide, which means that rapidly proliferating tissues are more sensitive to irradiation [68]. This is advantageous in cancer therapy as malignant cells tend to grow more rapidly than their corresponding normal cells. However, many normal tissues also exhibit a rapid turnover rate, such as bone marrow and intestinal epithelium, making them susceptible to acute effects of radiotherapy. As previously discussed, conventional RIT regimens may enable sufficient tumor targeting, but unfavorable pharmacokinetics result in too high absorbed doses to normal tissue, particularly to the bone marrow. Moreover, many common cancer types, such as breast and prostate, specifically metastasize to bone, which is problematic as acute myelotoxicity will limit all radiation therapy regimens. However, micrometastatic cells in the bone marrow are easily accessible for i.v. administered macromolecules [1], meaning that the possibility for efficient therapy is good as long as detrimental effects from nonspecific irradiation are reduced. This illustrates a common situation in which a successful systemic pretargeting strategy could enable better cure by delivering higher absorbed dose to the malignant cells while sparing the bone marrow.

This PhD project covers the development of a pretargeting system for ^{211}At therapy of disseminated cancer. The papers included describe progress from a preliminary *in vitro* model to i.p. therapy studies, and finally adaptation to i.v. conditions. The i.p. approach for PRIT of ovarian micrometastases is very interesting as the application of an intracavitary administration route inherently reduces some of the problems associated with systemic α-RIT, such as hematological toxicity and renal uptake. Still, the greatest gain of pretargeting may lie in systemic applications as it provides opportunities to improve survival rates of many different cancer types.

The design and execution of the *in vivo* studies in Paper II–IV have been limited by a number of factors, but one of the main difficulties was the production of sufficient amounts of high-quality (strept)avidin-antibody monomers. With low overall yields and occasionally irregular behavior (Paper IV), the availability of the pretargeting molecule has been of great concern. The amount of (S)Av-MX35 that has been administered in the animal studies (25–40 μg) has therefore been somewhat lower than desired for best possible saturation of available antigens. There are different ways to address this problem, either by improving the conjugation or by looking towards other modes of production, such as fusion protein technology. Hylarides et al. reported that the conjugate yield is directly influenced by the level of SMCC loading on (strept)avidin

[102]. They showed that a too low SMCC addition to SAv resulted in low yields because of decreased SAv consumption, while an overload of SMCC lead to increased SAv consumption but also formation of higher MW cross-linked species, thereby lowering the yields. A balance between conjugation efficiency and (S)Av-mAb monomer fraction requires optimization of this stoichiometry, as well as the applied reaction times. In our model (Paper I), this was done to a very limited degree, which could explain the low (S)Av-mAb production yields. Another reason for the meager outcome may be the small scale of our conjugation reactions, 100-fold lower than in some successful studies, as product is lost in each of the many purification steps [103]. The method could thus possibly be refined by the use of larger amounts of mAb.

Still, chemical conjugation methods are being surpassed by protein engineering techniques that generate tailored pretargeting molecules. Fully functional tetravalent fusion proteins of streptavidin and scFv fragments have been produced for many years [118-120]. Several preclinical studies [121-124] and a small number of clinical trials [125-127] demonstrated their use in pretargeting, and this method may ultimately prove to be a better option.

The availability of a suitable CA has been an impediment for the development of the pretargeting model for systemic applications. In the i.p. case, clearance of unbound pretargeting molecule was efficiently resolved by the glycosylated avidin, but for the i.v. model an additional agent was needed. The pretargeted distribution performed in Paper IV was facilitated by the generous donation of a small amount of NAGB from Dr. Oliver Press at the Fred Hutchinson Cancer Research Center in Seattle. Due to the limited supply of CA and SAv-MX35, no pilot studies were performed and the administration scheme was primarily based on data from Press et al. [44]. However, it is reasonable to suspect that there may be room for improvement of both tumor targeting and clearance with adjusted timing and dosage to better suit the pharmacokinetics of our particular model. An alternative method for clearance of unbound SAv-mAb is extracorporeal affinity adsorption (ECAT), in which blood is passed extracorporeally through a biotin-coated column. In a PRIT study by Mårtensson et al., ECAT was utilized for clearance of biotinylated antibodies before injection of radiolabeled streptavidin in rats. Tumor targeting was increased by 50%, and uptake in liver and lymph nodes reduced by 60% [128].

Other issues that have required significant time and attention in this project are the specific activity and stability of the ^{211}At-labeled effector molecule. Specific activity is a measurement of the fraction of molecules that carry an ^{211}At-atom. This plays an important role in the therapeutic outcome as saturation of pretargeted antigen sites by unlabeled effector molecules negatively affects the cumulated activity on the cell surface, thereby reducing the delivered absorbed dose [92]. The short half-life of ^{211}At and the low MW of the poly-L-lysine peptide used in Papers II–IV placed high demands on the labeling chemistry in order to reach sufficient specific activities for therapy. Despite short labeling times, radiolysis effects were troublesome when efforts were made to

label the m-MeATE-B-PL_{suc} conjugate with too high activities. In addition to poor radiochemical stability, detrimental effects on both the biotin moiety and the peptide itself were observed, resulting in low binding to avidin beads and aggregation to larger polymer complexes. A preliminary solution to the problem was reached by performing a series of similar labelings and pooling the resulting products, thus decreasing the total dose to the conjugate. In addition, non-conjugated succinylated poly-L-lysine was added to the reaction mix to reduce the radiation exposure of the m-MeATE-B-PL_{suc} conjugate. The i.p. and i.v. distributions of the resulting ^{211}At-B-PL_{suc} molecule both show that *in vivo* stability can be improved (Papers II and IV). The difference in uptake with and without the administration of sodium perchlorate to block free ^{211}At indicates that the radionuclide is released from the polymer backbone after passage through the kidneys. While blocking was efficient for most tissues, the lungs and spleen still showed elevated activity levels that could be problematic in terms of late radiation-induced effects. As anticipated for this low-MW effector molecule, renal uptake was also initially high, especially after systemic administration, but activity levels dropped rapidly, thereby limiting the absorbed dose. Renal toxicity is expected to manifest late, but the estimated absorbed doses from these biodistributions should be of no major concern, at least in terms of GFR.

A more disturbing finding was the unexpected accumulation in bone marrow, initially detected in the i.p. distributions and thereafter confirmed in the systemic study. At this point, little is known of this phenomenon; in what form the ^{211}At is distributed or why it accumulates in the RBM are undetermined. Neither do we know if it can be prevented by modifying the design of the effector molecule or by administrating of some kind of blocking agent. Because of the otherwise very promising results, especially considering the high and rapid tumor uptake demonstrated with systemic administration, efforts should be made to understand the mechanisms involved in the bone marrow uptake.

The tumor model for intraperitoneal ovarian micrometastases applied in the therapy study (Paper III) using i.p. inoculated NIH:OVCAR-3 cells has been used in a number of studies in Gothenburg over the years. Although the model has appeared to be stable, tumor growth in the inoculated animals was faster than expected, thereby causing a difficult starting point for the conducted therapies. The comparison between PRIT and conventional RIT suffered from this, as the amount of tumor cells was greater than anticipated in the design of the experiment, resulting in low probability of saturating the available antigen with the injected amount of radiolabeled molecules. Still, the resulting TFFs demonstrated efficacy for both approaches showing that cure may be possible also for animals with large tumor burden. In addition, proof-of-concept for i.p. PRIT was demonstrated. Comparison of therapeutic efficacy between ^{211}At-PRIT and ^{211}At-RIT in ascites-free animals nevertheless remains to be completed.

Although avidin and biotin has been used extensively for many kinds of biomolecular applications throughout the years, the decision to use the avidin–biotin system for pretargeting is not uncontroversial. The *in vivo* situation is associated with several

possible issues: immunogenicity of (strept)avidin, blocking by endogenous biotin, and the influence of a "binding-site barrier" resulting from the exceptionally strong interaction. Petronzelli et al. recently demonstrated that presence of anti-avidin antibodies, regardless of origin, does not affect the biotin-binding functions of avidin [129]. They also concluded that during 15 years of clinical use of avidin, including PRIT, no adverse events related to avidin immunogenicity have been reported. A few approaches for reducing the immune response to avidin and streptavidin have also been investigated, including polyethylene glycol modification and site-directed mutagenesis [130-132]. The results achieved so far are interesting but of preliminary nature. It should be pointed out that all patient populations are not equally prone to produce an antibody response. Diseases associated with inherent immunosuppression seem to affect the production of HAMA negatively, as observed, for instance, in patients with chronic lymphocytic leukemia [133, 134].

Presence of naturally occurring biotin in serum may interfere with (strept)avidin–biotin pretargeting strategies by competing with biotin-based or biotinylated effector molecules for binding to (strept)avidin-conjugated pretargeting molecules. The otherwise favorable high affinity becomes a problem if the biotin-binding sites are irreversibly occupied by endogenous biotin. Animals in preclinical studies can be provided with biotin-deficient feed to limit the biotin concentration in serum and tissues, but in human trials it is more difficult to control the presence of the vitamin. Several studies have therefore investigated the possibility of producing mutant streptavidin that enables both retained interaction with biotin-targeted molecules and lowered affinity for endogenous biotin. Results from preclinical studies proved this approach feasible together with designed biotin dimers, showing that potential issues caused by endogenous biotin can be overcome [135-138].

Although the importance of strong interaction between targeting molecules and tumor antigens has been emphasized throughout the years, a competing hypothesis stating that too strong interaction may lead to impaired tumor penetration has taken shape in parallel. The idea of a "binding-site barrier" effect is based on antibodies and other ligands binding with high affinity to the first encountered antigen on a tumor, thereby slowing intratumoral diffusion resulting in heterogeneous distribution [139-142]. Mathematical modeling has shown that a more uniform distribution may be reached by administering higher amounts of targeting molecules, thereby introducing more molecules available for penetration, but the downside is decreased specificity and less favorable TNTDR. Hypothetically, the strong interaction between (strept)avidin and biotin could cause similar problems with heterogeneous activity distribution in solid tumors after pretargeting, despite the small size of the radiolabeled effector molecules.

The accretion of radiolabeled molecules in tumors is influenced by many other factors, such as vascularization, intratumoral pressure, and antigen expression. Nonuniform activity distribution is a great problem for all RIT strategies, demanding higher doses for efficient cell killing. For RIT using α-particle emitters, the distribution is even more

important as the difference in required dose for equal surviving fraction between homogeneous and heterogeneous dose distributions is greater than for β-emitters, due to the lack of cross-fire effect [143]. In connection with the biodistributions described in Paper IV, a preliminary α-camera study was performed comparing the activity distribution in tumors after PRIT and RIT, with the hypothesis that pretargeting enables a more uniform dose distribution in shorter time compared with RIT. Figure 15 shows the results for three time points (0.5, 3, and 8 h p.i.). The distribution of the ^{211}At-labeled MX35 IgG followed the pattern for ^{211}At-MX35 F(ab')$_2$ previously described by Bäck and Jacobsson [112]. They observed very high activity in vascular compartments compared to surrounding tissue at 10 min p.i., after which high-activity patterns were visualized and identified as stromal compartments (7 h p.i.). A more uniform activity distribution was not seen until 21 h p.i. In this study, the distribution of ^{211}At-B-PL$_{suc}$ in the SAv-MX35-pretargeted tumors (7–10 mm) was remarkably uniform already at 30 min p.i. No interference from a "binding-site barrier" due to the strong streptavidin–biotin interaction was indicated. This therapeutically favorable outcome effectively demonstrates one of the main benefits of PRIT, especially for a short-lived α-particle emitter like ^{211}At.

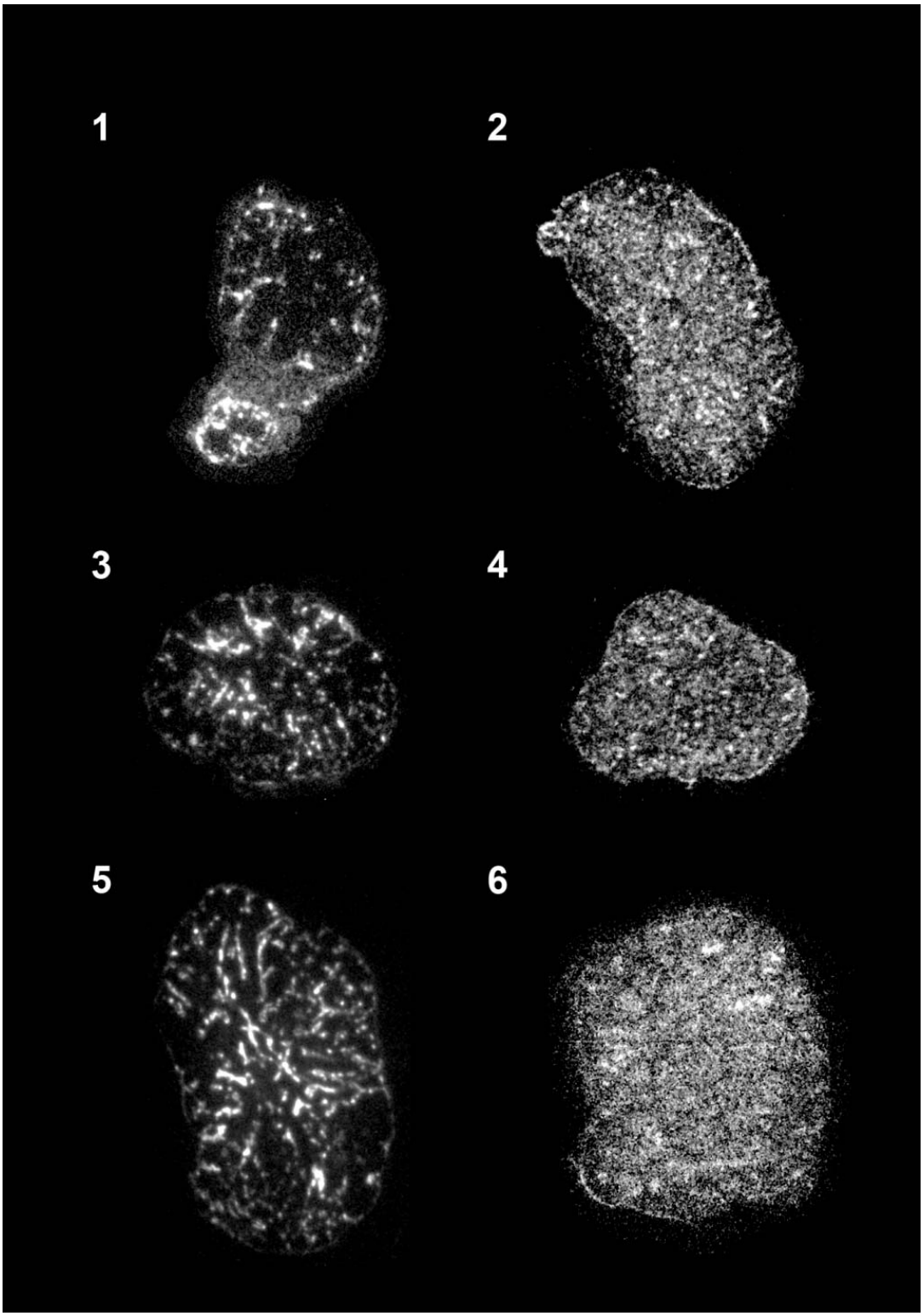

FIGURE 15. α-camera images showing the activity distribution in s.c. NIH:OVCAR-3 tumors (7–10 mm) at three different time points after i.v. injection of either ^{211}At-MX35 IgG (images 1, 3, and 5) or ^{211}At-B-PL$_{suc}$ (images 2, 4, and 6). Images 1 and 2 show the distribution at 30 min p.i., images 3 and 4 at 3 h p.i., and images 5 and 6 at 8 h p.i.

8.2 Future Work

The most important contribution deriving from this PhD project is the development of the ^{211}At-labeled, biotinylated, and succinylated poly-L-lysine-based effector molecule. The *in vivo* results reported in Papers II–IV show great promise for its use in pretargeted therapy regimens using the avidin–biotin system, but some questions remain that deserve more attention.

The polymeric framework allows great variation of the MW, an advantage of this molecule that has yet to be explored. Beginning with a somewhat larger poly-L-lysine base could lead to more favorable clearance as a result of the increase in net negative charge after succinylation, since a more anionic molecule would result in reduced renal filtration. This could decrease both uptake in the kidneys and the nonspecific accumulation of free ^{211}At that has been observed resulting from deastatination of the effector molecule. In addition, it may affect the unfavorable localization of ^{211}At in the bone marrow. The α-camera technique is an extremely valuable tool that can be used for investigating the effect of altered MW. Comparing the activity distribution in sections of tumors and normal tissues for different sizes of poly-L-lysine would be a sophisticated method for optimization of the TNTDR after pretargeting. Different bonding agents for astatination of the biotinylated poly-L-lysine molecule could also be investigated, such as boron cage moieties, which may increase the stability of the ^{211}At-labeled product.

Another appealing course is to evaluate the ^{211}At-labeled peptide in other tumor models, besides the ovarian carcinoma model described in this thesis. There are several hematologic tumor models for which streptavidin–biotin pretargeting has been successfully applied, to which this effector molecule easily could be adapted. For instance, in the treatment of multiple myeloma or AML the observed uptake in RBM does not have to be disadvantageous, as the targeted malignant cells are situated in the bone marrow.

For many years the general consensus regarding α-emitters in RIT of solid tumors has been that their primary use will be treatment of micrometastases and residual disease. Unfavorable absorbed dose distributions have precluded α-RIT of macroscopic tumors, but with successful pretargeting this paradigm may no longer be true. We demonstrated that a uniform activity distribution was achievable in solid tumors after merely 30 min using the pretargeting system developed in this project in a pilot α-camera study. These preliminary results certainly encourage further studies of systemic ^{211}At-PRIT to evaluate the possibility of efficient eradication not only of microscopic but also macroscopic tumors without the detrimental effects on normal tissue.

ACKNOWLEDGEMENTS

Throughout my time as a doctoral student I have always considered myself incredibly fortunate; I have had the opportunity to be advised by not just one but three great scientific minds. Not once have I been in need of counsel without receiving it, no matter what the issue. For that I am most grateful.

My greatest of thanks goes to my main supervisor **Sture Lindegren**. Your never-ending enthusiasm and willingness to try new things is truly inspiring, and I hope that some of your chaotic intellect has rubbed off on me. Together we have made a good team of chemists supplementing one another, in the lab as well as in the writing process. I have had a lot of fun working with you and hope that our collaboration will persist for many years to come!

As head of the astatine group, my assistant supervisor **Lars Jacobsson** has been a sound pillar, always making sure that our research lives up to high scientific and ethical standards. Your calm advice and pedagogical dosimetry tutoring have been invaluable to me, and I have much appreciated our (sometimes lengthy) Friday meetings. Thank you!

Another wholehearted and inspiring force of nature is my other assistant advisor **Ragnar Hultborn**. Meetings with you are never boring, and ideas blow in from every direction. I am very grateful for the time you have spent with me, looking at microscope slides and discussing manuscripts.

Another person to whom great appreciation is due is **Tom Bäck**. Working closely with you has affected me in so many ways; you have shared your experimental skills, your scientific spark, your passion for music and art, your fondness of running, and last but not least, your friendship. Without you, work would have been much more dull (and lacking those stunning α-camera images…).

Helena Kahu is humbly acknowledged for her important contributions to basically all my experiments, *in vitro* and *in vivo*. Thanks are also due to **Jörgen Elgqvist**, **Elisabet Warnhammar**, and **Ulla Delle** for kind and skillful support. **Nicolas Chouin** deserves a bottle of good French wine for putting up with the α-camera night shifts and for his patience with my dosimetry questions. Heartfelt appreciation goes out to my roommate and long-time companion **Elin Cederkrantz**, for being my friend practically from my first day in Gothenburg. I would also like to express my sincere gratitude to the rest of the targeted alpha therapy (TAT) group, for fun times and good collaboration, especially **Anna Gustafsson**, **Stig Palm**, **Per Albertsson**, **Håkan Andersson**, and **Holger Jensen**.

Warm thanks go out to all colleagues, friends, and fellow PhD students at the Department of Radiation Physics and the Department of Medical Physics and Biomedical Engineering for interesting discussions and lots of laughs, both on and off work; especially **Nils Rudqvist**, **Anders Josefsson**, **Maria Larsson**, **Jenny Nilsson**, and **Emilia Runge**. **Niclas Pettersson** deserves particular recognition for his support during this last year, persistently telling me to be kind to myself.

And then there are all the people outside of work… Sincere appreciation goes to **Sofia** and **Martin** who picked me up when I was at the bottom, brushed off the dirt and made sure that I got up on my feet again. Such kindness is rare! My dear friends **Patrik** and **Tomas** are also acknowledged for their fine companionship, through thick and thin.

A much-loved circle of friends from Halmstad must also be mentioned: **Diana**, **Karin**, **Tilda**, and **Vivi**. I hope that we will keep on sharing all of life's experiences, both good and bad. With you, tears of sorrow are always mixed with tears of joy.

Lastly, all my love to my family. Naturally, I owe everything to my parents, **Göran** and **Barbro**. You may not realize it but all that I am proud of in myself, I got from you. I gratefully acknowledge my sister **Johanna** and her family for always welcoming me in their warm home. And finally there is my brother **Anton**, who kindly let his kid sister stumble in his footsteps from childhood to Chalmers. The funniest, most intelligent, and headstrong person I know – forever my idol.

♥

Financial support from the Swedish Cancer Society, the King Gustaf V Jubilee Clinic Research Foundation, the Swedish Research Council, The Foundation Assar Gabrielsson for Clinical Research, and the Sahlgrenska University Hospital Foundations is gratefully acknowledged.

REFERENCES

1. Pantel, K., R.J. Cote, and Ø. Fodstad, *Detection and clinical importance of micrometastatic disease.* J Natl Cancer Inst, 1999. **91**(13): p. 1113-1124.
2. Chambers, A.F., A.C. Groom, and I.C. MacDonald, *Metastasis: Dissemination and growth of cancer cells in metastatic sites.* Nat Rev Cancer, 2002. **2**(8): p. 563-572.
3. Strebhardt, K. and A. Ullrich, *Paul Ehrlich's magic bullet concept: 100 years of progress.* Nat Rev Cancer, 2008. **8**(6): p. 473-480.
4. Imai, K. and A. Takaoka, *Comparing antibody and small-molecule therapies for cancer.* Nat Rev Cancer, 2006. **6**(9): p. 714-727.
5. Köhler, G. and C. Milstein, *Continuous cultures of fused cells secreting antibody of predefined specificity.* Nature, 1975. **256**(5517): p. 495-497.
6. Kricka, L.J., *Human anti-animal antibody interferences in immunological assays.* Clin Chem, 1999. **45**(7): p. 942-956.
7. Hoogenboom, H.R. and P. Chames, *Natural and designer binding sites made by phage display technology.* Immunol Today, 2000. **21**(8): p. 371-378.
8. Adams, G.P. and L.M. Weiner, *Monoclonal antibody therapy of cancer.* Nat Biotechnol, 2005. **23**(9): p. 1147-57.
9. Huhalov, A. and K.A. Chester, *Engineered single chain antibody fragments for radioimmunotherapy.* Q J Nucl Med Mol Imaging, 2004. **48**(4): p. 279-88.
10. Nord, K., et al., *Binding proteins selected from combinatorial libraries of an [alpha]-helical bacterial receptor domain.* Nat Biotechnol, 1996. **15**(8): p. 772-777.
11. Wu, A.M. and P.D. Senter, *Arming antibodies: prospects and challenges for immunoconjugates.* Nat Biotechnol, 2005. **23**(9): p. 1137-1146.
12. Smith, M.R., *Rituximab (monoclonal anti-CD20 antibody): mechanisms of action and resistance.* Oncogene, 2003. **22**(47): p. 7359-7368.
13. Nahta, R. and F.J. Esteva, *Herceptin: mechanisms of action and resistance.* Cancer Lett, 2006. **232**(2): p. 123-38.
14. Jonker, D.J., et al., *Cetuximab for the treatment of colorectal cancer.* N Engl J Med, 2007. **357**(20): p. 2040-2048.
15. Ferrara, N., K.J. Hillan, and W. Novotny, *Bevacizumab (Avastin), a humanized anti-VEGF monoclonal antibody for cancer therapy.* Biochem Biophys Res Commun, 2005. **333**(2): p. 328-335.
16. Goldenberg, D.M., et al., *Experimental radioimmunotherapy of a xenografted human colonic tumor (GW-39) producing carcinoembryonic antigen.* Cancer Res, 1981. **41**(11 Part 1): p. 4354-4360.
17. Goldenberg, D.M., *Targeted therapy of cancer with radiolabeled antibodies.* J Nucl Med, 2002. **43**(5): p. 693-713.
18. Goldenberg, D.M., *Advancing role of radiolabeled antibodies in the therapy of cancer.* Cancer Immunol Immunother, 2003. **52**(5): p. 281-96.
19. Wang, W., E.Q. Wang, and J.P. Balthasar, *Monoclonal antibody pharmacokinetics and pharmacodynamics.* Clin Pharmacol Ther, 2008. **84**(5): p. 548-558.
20. Witzig, T.E., et al., *Randomized controlled trial of yttrium-90–labeled ibritumomab tiuxetan radioimmunotherapy versus rituximab immunotherapy for patients with relapsed or refractory low-grade, follicular, or transformed B-cell non-Hodgkin's lymphoma.* J Clin Oncol, 2002. **20**(10): p. 2453-2463.
21. Kaminski, M.S., et al., *Radioimmunotherapy with iodine 131I tositumomab for relapsed or refractory B-cell non-Hodgkin lymphoma: updated results and long-term follow-up of the University of Michigan experience.* Blood, 2000. **96**(4): p. 1259-1266.
22. Andersson, H., et al., *Intraperitoneal α-particle radioimmunotherapy of ovarian cancer patients: pharmacokinetics and dosimetry of 211At-MX35 F(ab')2–a phase I study.* J Nucl Med, 2009: p. 1153-1160.

23. Zalutsky, M.R., et al., *Clinical experience with alpha-particle emitting 211At: treatment of recurrent brain tumor patients with 211At-labeled chimeric antitenascin monoclonal antibody 81C6.* J Nucl Med, 2008. **49**(1): p. 30-8.
24. Boerman, O.C., et al., *Pretargeted radioimmunotherapy of cancer: progress step by step.* J Nucl Med, 2003. **44**(3): p. 400-11.
25. Goldenberg, D.M., et al., *Antibody pretargeting advances cancer radioimmunodetection and radioimmunotherapy.* J Clin Oncol, 2006. **24**(5): p. 823-34.
26. Reardan, D.T., et al., *Antibodies against metal chelates.* Nature, 1985. **316**(6025): p. 265-268.
27. Goodwin, D.A., et al., *Monoclonal antibodies as reversible equilibrium carriers of radiopharmaceuticals.* Int J Radiat Appl Instrum B, 1986. **13**(4): p. 383-391.
28. Goodwin, D.A., et al., *Pre-targeted immunoscintigraphy of murine tumors with indium-111-labeled bifunctional haptens.* J Nucl Med, 1988. **29**(2): p. 226-34.
29. Stickney, D.R., et al., *Bifunctional antibody: a binary radiopharmaceutical delivery system for imaging colorectal carcinoma.* Cancer Res, 1991. **51**(24): p. 6650-5.
30. Le Doussal, J.-M., et al., *In vitro and in vivo targeting of radiolabeled monovalent and divalent haptens with dual specificity monoclonal antibody conjugates: enhanced divalent hapten affinity for cell-bound antibody conjugate.* J Nucl Med, 1989. **30**(8): p. 1358-1366.
31. Barbet, J., et al., *Pretargeting with the affinity enhancement system for radioimmunotherapy.* Cancer Biother Radiopharm, 1999. **14**(3): p. 153-66.
32. Sakahara, H. and T. Saga, *Avidin-biotin system for delivery of diagnostic agents.* Adv Drug Deliv Rev, 1999. **37**(1-3): p. 89-101.
33. Lesch, H.P., et al., *Avidin-biotin technology in targeted therapy.* Expert Opin Drug Deliv, 2010. **7**(5): p. 551-64.
34. Hnatowich, D.J., F. Virzi, and M. Rusckowski, *Investigations of avidin and biotin for imaging applications.* J Nucl Med, 1987. **28**(8): p. 1294-302.
35. Sung, C. and W.W. van Osdol, *Pharmacokinetic comparison of direct antibody targeting with pretargeting protocols based on streptavidin-biotin binding.* J Nucl Med, 1995. **36**(5): p. 867-76.
36. Kalofonos, H.P., et al., *Imaging of tumor in patients with indium-111-labeled biotin and streptavidin-conjugated antibodies: preliminary communication.* J Nucl Med, 1990. **31**(11): p. 1791-1796.
37. Paganelli, G., et al., *Two-step tumour targetting in ovarian cancer patients using biotinylated monoclonal antibodies and radioactive streptavidin.* Eur J Nucl Med Mol Imaging, 1992. **19**(5): p. 322-329.
38. Paganelli, G., et al., *Three-step monoclonal antibody tumor targeting in carcinoembryonic antigen-positive patients.* Cancer Res, 1991. **51**(21): p. 5960-6.
39. Paganelli, G., et al., *Antibody-guided three-step therapy for high grade glioma with yttrium-90 biotin.* Eur J Nucl Med, 1999. **26**(4): p. 348-57.
40. Grana, C., et al., *Pretargeted adjuvant radioimmunotherapy with yttrium-90-biotin in malignant glioma patients: a pilot study.* Br J Cancer, 2002. **86**(2): p. 207-212.
41. Axworthy, D.B., et al., *Cure of human carcinoma xenografts by a single dose of pretargeted yttrium-90 with negligible toxicity.* Proc Natl Acad Sci USA, 2000. **97**(4): p. 1802-7.
42. Breitz, H.B., et al., *Clinical optimization of pretargeted radioimmunotherapy with antibody-streptavidin conjugate and 90Y-DOTA-biotin.* J Nucl Med, 2000. **41**(1): p. 131-40.
43. Knox, S.J., et al., *Phase II trial of yttrium-90-DOTA-biotin pretargeted by NR-LU-10 antibody/streptavidin in patients with metastatic colon cancer.* Clin Cancer Res, 2000. **6**(2): p. 406-14.
44. Press, O.W., et al., *A comparative evaluation of conventional and pretargeted radioimmunotherapy of CD20-expressing lymphoma xenografts.* Blood, 2001. **98**(8): p. 2535-43.
45. Weiden, P.L. and H.B. Breitz, *Pretargeted radioimmunotherapy (PRIT) for treatment of non-Hodgkin's lymphoma (NHL).* Crit Rev Oncol Hematol, 2001. **40**(1): p. 37-51.

46. Park, S.I., et al., *Conventional and pretargeted radioimmunotherapy using bismuth-213 to target and treat non-Hodgkin lymphomas expressing CD20: a preclinical model toward optimal consolidation therapy to eradicate minimal residual disease.* Blood, 2010. **116**(20): p. 4231-4239.
47. Palanca-Wessels, M.C.A. and O.W. Press, *Improving the efficacy of radioimmunotherapy for non-Hodgkin lymphomas.* Cancer, 2010. **116**(4): p. 1126-1133.
48. Pagel, J.M., et al., *Comparison of anti-CD20 and anti-CD45 antibodies for conventional and pretargeted radioimmunotherapy of B-cell lymphomas.* Blood, 2003. **101**(6): p. 2340-8.
49. Pagel, J.M., et al., *Eradication of disseminated leukemia in a syngeneic murine leukemia model using pretargeted anti-CD45 radioimmunotherapy.* Blood, 2008. **111**(4): p. 2261-2268.
50. Zhang, M., et al., *Pretargeting radioimmunotherapy of a murine model of adult T-cell leukemia with the alpha-emitting radionuclide, bismuth 213.* Blood, 2002. **100**(1): p. 208-16.
51. Zhang, M., et al., *Pretarget radiotherapy with an anti-CD25 antibody-streptavidin fusion protein was effective in therapy of leukemia/lymphoma xenografts.* Proc Natl Acad Sci USA, 2003. **100**(4): p. 1891-5.
52. Pagel, J.M., et al., *Anti-CD45 pretargeted radioimmunotherapy using bismuth-213: high rates of complete remission and long-term survival in a mouse myeloid leukemia xenograft model.* Blood, 2011. **118**(3): p. 703-711.
53. Wang, Y., et al., *Pretargeting with amplification using polymeric peptide nucleic acid.* Bioconjug Chem, 2001. **12**(5): p. 807-16.
54. He, J., et al., *Amplification targeting: a modified pretargeting approach with potential for signal amplification—proof of a concept.* J Nucl Med, 2004. **45**(6): p. 1087-1095.
55. Kuijpers, W.H., et al., *Specific recognition of antibody-oligonucleotide conjugates by radiolabeled antisense nucleotides: a novel approach for two-step radioimmunotherapy of cancer.* Bioconjug Chem, 1993. **4**(1): p. 94-102.
56. Rusckowski, M., et al., *Pretargeting using peptide nucleic acid.* Cancer, 1997. **80**(12 Suppl): p. 2699-705.
57. Mang'era, K., et al., *Initial investigations of 99mTc-labeled morpholinos for radiopharmaceutical applications.* Eur J Nucl Med Mol Imaging, 2001. **28**(11): p. 1682-1689.
58. Liu, G., et al., *Tumor pretargeting in mice using (99m)Tc-labeled morpholino, a DNA analog.* J Nucl Med, 2002. **43**(3): p. 384-91.
59. Liu, G., et al., *Pretargeting CWR22 prostate tumor in mice with MORF-B72.3 antibody and radiolabeled cMORF.* Eur J Nucl Med Mol Imaging, 2008. **35**(2): p. 272-80.
60. He, J., et al., *Affinity enhancement bivalent morpholino for pretargeting: initial evidence by surface plasmon resonance.* Bioconjug Chem, 2005. **16**(2): p. 338-345.
61. He, J., et al., *Affinity enhancement bivalent morpholinos for pretargeting: surface plasmon resonance studies of molecular dimensions.* Bioconjug Chem, 2005. **16**(5): p. 1098-1104.
62. Chmura, A.J., M.S. Orton, and C.F. Meares, *Antibodies with infinite affinity.* Proc Natl Acad Sci USA, 2001. **98**(15): p. 8480-8484.
63. Wei, L.H., et al., *Engineered antibody fragments with infinite affinity as reporter genes for PET imaging.* J Nucl Med, 2008. **49**(11): p. 1828-1835.
64. Cherel, M., et al., *Current status and perspectives in alpha radioimmunotherapy.* Q J Nucl Med Mol Imaging, 2006. **50**(4): p. 322-329.
65. Weber, K.J. and M. Flentje, *Lethality of heavy ion-induced DNA double-strand breaks in mammalian cells.* Int J Radiat Biol, 1993. **64**(2): p. 169-178.
66. Kassis, A.I., *Therapeutic radionuclides: biophysical and radiobiologic principles.* Semin Nucl Med, 2008. **38**(5): p. 358-66.
67. Sgouros, G., *Alpha-particles for targeted therapy.* Adv Drug Deliv Rev, 2008. **60**(12): p. 1402-6.
68. Hall, E.J., *Radiobiology for the radiologist*. 5th ed. 2000, Philadelphia, PA: Lippincott Williams & Wilkins.

69. Govindan, S.V., et al., *Yttrium-90-labeled complementarity-determining-region-grafted monoclonal antibodies for radioimmunotherapy: radiolabeling and animal biodistribution studies.* Bioconjug Chem, 1998. **9**(6): p. 773-782.
70. Wilbur, D.S., *Chemical and radiochemical considerations in radiolabeling with alpha-emitting radionuclides.* Curr Radiopharm, 2011. **4**(3): p. 214-47.
71. McDevitt, M.R., et al., *Radioimmunotherapy with alpha-emitting nuclides.* Eur J Nucl Med, 1998. **25**(9): p. 1341-51.
72. Atcher, R.W., A.M. Friedman, and J.J. Hines, *An improved generator for the production of 212Pb and 212Bi from 224Ra.* Int J Radiat Appl Instrum Appl Radiat Isot, 1988. **39**(4): p. 283-286.
73. Ma, D., et al., *Breakthrough of 225Ac and its radionuclide daughters from an 225Ac/213Bi generator: development of new methods, quantitative characterization, and implications for clinical use.* Appl Radiat Isot, 2001. **55**(5): p. 667-678.
74. Larsen, R.H., B.W. Wieland, and M.R. Zalutsky, *Evaluation of an internal cyclotron target for the production of 211At via the 209Bi (α,2n)211At reaction.* Appl Radiat Isot, 1996. **47**(2): p. 135-143.
75. O'Donoghue, J.A., M. Bardiès, and T.E. Wheldon, *Relationships between tumor size and curability for uniformly targeted therapy with beta-emitting radionuclides.* J Nucl Med, 1995. **36**(10): p. 1902-1909.
76. Zalutsky, M.R. and M. Pruszynski, *Astatine-211: production and availability.* Curr Radiopharm, 2011. **4**(3): p. 177-85.
77. Wilbur, D.S., et al., *Preparation and evaluation of para-[211At]astatobenzoyl labeled anti-renal cell carcinoma antibody A6H F(ab')2. In vivo distribution comparison with para-[125I]iodobenzoyl labeled A6H F(ab')2.* Nucl Med Biol, 1993. **20**(8): p. 917-927.
78. Lindegren, S., T. Bäck, and H.J. Jensen, *Dry-distillation of astatine-211 from irradiated bismuth targets: a time-saving procedure with high recovery yields.* Appl Radiat Isot, 2001. **55**(2): p. 157-60.
79. Visser, G.W.M., E.L. Diemer, and F.M. Kaspersen, *The nature of the astatine-protein bond.* Int J Appl Radiat Isot, 1981. **32**(12): p. 905-912.
80. Wilbur, D.S., *Radiohalogenation of proteins: An overview of radionuclides, labeling methods and reagents for conjugate labeling.* Bioconjug Chem, 1992. **3**(6): p. 433-470.
81. Corson, D.R., K.R. MacKenzie, and E. Segrè, *Artificially radioactive element 85.* Phys Rev, 1940. **58**(8): p. 672-678.
82. Wilbur, D.S., et al., *Reagents for astatination of biomolecules: comparison of the in vivo distribution and stability of some radioiodinated/astatinated benzamidyl and nido-carboranyl compounds.* Bioconjug Chem, 2004. **15**(1): p. 203-23.
83. Wilbur, D.S., et al., *Reagents for astatination of biomolecules. 2. Conjugation of anionic boron cage pendant groups to a protein provides a method for direct labeling that is stable to in vivo deastatination.* Bioconjug Chem, 2007. **18**(4): p. 1226-40.
84. Zalutsky, M.R. and A.S. Narula, *Astatination of proteins using an N-succinimidyl tri-n-butylstannyl benzoate intermediate.* Int J Radiat Appl Instrum Appl Radiat Isot, 1988. **39**(3): p. 227-232.
85. Garg, P.K., et al., *Synthesis of radioiodinated N-succinimidyl iodobenzoate: optimization for use in antibody labelling.* Int J Radiat Appl Instrum Appl Radiat Isot, 1989. **40**(6): p. 485-490.
86. Wilbur, D.S., et al., *Development of a stable radioiodinating reagent to label monoclonal antibodies for radiotherapy of cancer.* J Nucl Med, 1989. **30**(2): p. 216-26.
87. Lindegren, S., et al., *Direct procedure for the production of 211At-labeled antibodies with an epsilon-lysyl-3-(trimethylstannyl)benzamide immunoconjugate.* J Nucl Med, 2008. **49**(9): p. 1537-45.
88. Jaaback, K., N. Johnson, and A. Lawrie Theresa (2011) *Intraperitoneal chemotherapy for the initial management of primary epithelial ovarian cancer*. Cochrane Database Syst Rev, DOI: 10.1002/14651858.CD005340.pub3.

89. Andersson, H., et al., *The curative and palliative potential of the monoclonal antibody MOv18 labelled with 211At in nude mice with intraperitoneally growing ovarian cancer xenografts–a long-term study.* Acta Oncol, 2000. **39**(6): p. 741-5.
90. Andersson, H., et al., *Radioimmunotherapy of nude mice with intraperitoneally growing ovarian cancer xenograft utilizing At-211-labelled monoclonal antibody MOv18.* Anticancer Res, 2000. **20**(1A): p. 459-462.
91. Andersson, H., et al., *Comparision of the therapeutic efficacy of At-211- and I-131-labelled monoclonal antibody MOv18 in nude mice with intraperitoneal growth of human ovarian cancer.* Anticancer Res, 2001. **21**(1A): p. 409-412.
92. Elgqvist, J., et al., *Therapeutic efficacy and tumor dose estimations in radioimmunotherapy of intraperitoneally growing OVCAR-3 cells in nude mice with (211)At-labeled monoclonal antibody MX35.* J Nucl Med, 2005. **46**(11): p. 1907-15.
93. Elgqvist, J., et al., *Alpha-radioimmunotherapy of intraperitoneally growing OVCAR-3 tumors of variable dimensions: outcome related to measured tumor size and mean absorbed dose.* J Nucl Med, 2006. **47**(8): p. 1342-50.
94. Elgqvist, J., et al., *Administered activity and metastatic cure probability during radioimmunotherapy of ovarian cancer in nude mice with (211)At-MX35 F(ab')(2).* Int J Radiat Oncol Biol Phys, 2006. **66**(4): p. 1228-37.
95. Elgqvist, J., et al., *Fractionated radioimmunotherapy of intraperitoneally growing ovarian cancer in nude mice with 211At-MX35 F(ab')2: therapeutic efficacy and myelotoxicity.* Nucl Med Biol, 2006. **33**(8): p. 1065-72.
96. Felip, E., et al., *Overexpression of c-erbB-2 in epithelial ovarian cancer. Prognostic value and relationship with response to chemotherapy.* Cancer, 1995. **75**(8): p. 2147-2152.
97. Yin, B.W., et al., *Monoclonal antibody MX35 detects the membrane transporter NaPi2b (SLC34A2) in human carcinomas.* Cancer Immun, 2008. **8**: p. 3.
98. Palm, S., et al., *Therapeutic efficacy of astatine-211-labeled trastuzumab on radioresistant SKOV-3 tumors in nude mice.* Int J Radiat Oncol Biol Phys, 2007. **69**(2): p. 572-9.
99. Hamilton, T.C., et al., *Characterization of a xenograft model of human ovarian carcinoma which produces ascites and intraabdominal carcinomatosis in mice.* Cancer Res, 1984. **44**(11): p. 5286-5290.
100. Karacay, H., et al., *Development of a streptavidin-anti-carcinoembryonic antigen antibody, radiolabeled biotin pretargeting method for radioimmunotherapy of colorectal cancer. Reagent development.* Bioconjug Chem, 1997. **8**(4): p. 585-94.
101. Foulon, C.F., D.D. Bigner, and M.R. Zalutsky, *Preparation and characterization of anti-tenascin monoclonal antibody-streptavidin conjugates for pretargeting applications.* Bioconjug Chem, 1999. **10**(5): p. 867-76.
102. Hylarides, M.D., R.W. Mallett, and D.L. Meyer, *A robust method for the preparation and purification of antibody/streptavidin conjugates.* Bioconjug Chem, 2001. **12**(3): p. 421-7.
103. Jia, F., T.D. Shelton, and M.R. Lewis, *Preparation, characterization, and biological evaluation of a streptavidin-chimeric t84.66 conjugate for antibody pretargeting.* Cancer Biother Radiopharm, 2007. **22**(5): p. 654-64.
104. Lindmo, T., et al., *Determination of the immunoreactive fraction of radiolabeled monoclonal antibodies by linear extrapolation to binding at infinite antigen excess.* J Immunol Methods, 1984. **72**(1): p. 77-89.
105. Foulon, C.F., B.W. Schoultz, and M.R. Zalutsky, *Preparation and biological evaluation of an astatine-211 labeled biotin conjugate: biotinyl-3-[211 At]astatoanilide.* Nucl Med Biol, 1997. **24**(2): p. 135-43.
106. Wilbur, D.S., et al., *Biotin reagents in antibody pretargeting. 6. Synthesis and in vivo evaluation of astatinated and radioiodinated aryl- and nido-carboranyl-biotin derivatives.* Bioconjug Chem, 2004. **15**(3): p. 601-616.
107. Wilbur, D.S., *[211At]astatine-labeled compound stability: Issues with released [211At]astatide and development of labeling reagents to increase stability.* Curr Radiopharm, 2008. **1**(3): p. 144-176.

108. Torchilin, V.P., et al., *Monoclonal antibody modification with chelate-linked high-molecular-weight polymers: major increases in polyvalent cation binding without loss of antigen binding.* Hybridoma, 1987. **6**(3): p. 229-40.
109. del Rosario, R.B. and R.L. Wahl, *Biotinylated iodo-polylysine for pretargeted radiation delivery.* J Nucl Med, 1993. **34**(7): p. 1147-51.
110. Lindegren, S., et al., *Synthesis and biodistribution of 211At-labeled, biotinylated, and charge-modified poly-L-lysine: evaluation for use as an effector molecule in pretargeted intraperitoneal tumor therapy.* Bioconjug Chem, 2002. **13**(3): p. 502-9.
111. Lindegren, S., et al., *(211)At-labeled and biotinylated effector molecules for pretargeted radioimmunotherapy using poly-L- and poly-D-Lysine as multicarriers.* Clin Cancer Res, 2003. **9**(10 Pt 2): p. 3873S-9S.
112. Bäck, T. and L. Jacobsson, *The alpha-camera: a quantitative digital autoradiography technique using a charge-coupled device for ex vivo high-resolution bioimaging of alpha-particles.* J Nucl Med, 2010. **51**(10): p. 1616-23.
113. Chouin, N., et al., *Evidence of extranuclear cell sensitivity to alpha-particle radiation using a microdosimetric model. I. Presentation and validation of a microdosimetric model.* Radiat Res, 2009. **171**(6): p. 657-63.
114. Bäck, T., et al., *Glomerular filtration rate after alpha-radioimmunotherapy with At-211-MX35-F(ab')(2): a long-term study of renal function in nude mice.* Cancer Biother Radiopharm, 2009. **24**(6): p. 649-658.
115. Larsen, R.H., S. Slade, and M.R. Zalutsky, *Blocking [211At]astatide accumulation in normal tissues: preliminary evaluation of seven potential compounds.* Nucl Med Biol, 1998. **25**(4): p. 351-7.
116. Elgqvist, J., et al., *Myelotoxicity and RBE of 211At-conjugated monoclonal antibodies compared with 99mTc-conjugated monoclonal antibodies and 60Co irradiation in nude mice.* J Nucl Med, 2005. **46**(3): p. 464-71.
117. Bäck, T., et al., *211At radioimmunotherapy of subcutaneous human ovarian cancer xenografts: evaluation of relative biologic effectiveness of an alpha-emitter in vivo.* J Nucl Med, 2005. **46**(12): p. 2061-7.
118. Dübel, S., et al., *Bifunctional and multimeric complexes of streptavidin fused to single chain antibodies (scFv).* J Immunol Methods, 1995. **178**(2): p. 201-209.
119. Schultz, J., et al., *A tetravalent single-chain antibody-streptavidin fusion protein for pretargeted lymphoma therapy.* Cancer Res, 2000. **60**(23): p. 6663-9.
120. Wang, W.W., et al., *Design of a bifunctional fusion protein for ovarian cancer drug delivery: single-chain anti-CA125 core-streptavidin fusion protein.* Eur J Pharm Biopharm, 2007. **65**(3): p. 398-405.
121. Goshorn, S., et al., *Preclinical evaluation of a humanized NR-LU-10 antibody-streptavidin fusion protein for pretargeted cancer therapy.* Cancer Biother Radiopharm, 2001. **16**(2): p. 109-23.
122. Buchsbaum, D.J., et al., *Intraperitoneal pretarget radioimmunotherapy with CC49 fusion protein.* Clin Cancer Res, 2005. **11**(22): p. 8180-5.
123. Pagel, J.M., et al., *Comparison of a tetravalent single-chain antibody-streptavidin fusion protein and an antibody-streptavidin chemical conjugate for pretargeted anti-CD20 radioimmunotherapy of B-cell lymphomas.* Blood, 2006. **108**(1): p. 328-336.
124. Green, D.J., et al., *Pretargeting CD45 enhances the selective delivery of radiation to hematolymphoid tissues in nonhuman primates.* Blood, 2009. **114**(6): p. 1226-1235.
125. Forero, A., et al., *Phase 1 trial of a novel anti-CD20 fusion protein in pretargeted radioimmunotherapy for B-cell non-Hodgkin lymphoma.* Blood, 2004. **104**(1): p. 227-36.
126. Shen, S., et al., *Patient-specific dosimetry of pretargeted radioimmunotherapy using CC49 fusion protein in patients with gastrointestinal malignancies.* J Nucl Med, 2005. **46**(4): p. 642-51.
127. Forero-Torres, A., et al., *Pretargeted radioimmunotherapy (RIT) with a novel anti-TAG-72 fusion protein.* Cancer Biother Radiopharm, 2005. **20**(4): p. 379-90.

128. Mårtensson, L., et al., *Improved tumor targeting and decreased normal tissue accumulation through extracorporeal affinity adsorption in a two-step pretargeting strategy.* Clin Cancer Res, 2007. **13**(18 Pt 2): p. 5572s-5576s.
129. Petronzelli, F., et al., *Therapeutic use of avidin is not hampered by antiavidin antibodies in humans.* Cancer Biother Radiopharm, 2010. **25**(5): p. 563-70.
130. Marshall, D., et al., *Polyethylene glycol modification of a galactosylated streptavidin clearing agent: effects on immunogenicity and clearance of a biotinylated anti-tumour antibody.* Br J Cancer, 1996. **73**(5): p. 565-572.
131. Caliceti, P., et al., *Poly(ethylene glycol)-avidin bioconjugates: suitable candidates for tumor pretargeting.* J Control Release, 2002. **83**(1): p. 97-108.
132. Meyer, D.L., et al., *Reduced antibody response to streptavidin through site-directed mutagenesis.* Protein Sci, 2001. **10**(3): p. 491-503.
133. Schroff, R.W., et al., *Human anti-murine immunoglobulin responses in patients receiving monoclonal antibody therapy.* Cancer Res, 1985. **45**(2): p. 879-885.
134. Shawler, D., et al., *Human immune response to multiple injections of murine monoclonal IgG.* J Immunol, 1985. **135**(2): p. 1530-1535.
135. Hamblett, K.J., et al., *A streptavidin-biotin binding system that minimizes blocking by endogenous biotin.* Bioconjug Chem, 2002. **13**(3): p. 588-98.
136. Hamblett, K.J., et al., *Role of biotin-binding affinity in streptavidin-based pretargeted radioimmunotherapy of lymphoma.* Bioconjug Chem, 2005. **16**(1): p. 131-138.
137. Wilbur, D.S., et al., *Design and synthesis of bis-biotin-containing reagents for applications utilizing monoclonal antibody-based pretargeting systems with streptavidin mutants.* Bioconjug Chem, 2010. **21**(7): p. 1225-1238.
138. Park, S.I., et al., *Pretargeted radioimmunotherapy using genetically engineered antibody-streptavidin fusion proteins for treatment of non-Hodgkin lymphoma.* Clin Cancer Res, 2011. **17**(23): p. 7373-82.
139. Fujimori, K., et al., *A modeling analysis of monoclonal antibody percolation through tumors: a binding-site barrier.* J Nucl Med, 1990. **31**(7): p. 1191-1198.
140. van Osdol, W., K. Fujimori, and J.N. Weinstein, *An analysis of monoclonal antibody distribution in microscopic tumor nodules: consequences of a "binding site barrier".* Cancer Res, 1991. **51**(18): p. 4776-4784.
141. Juweid, M., et al., *Micropharmacology of monoclonal antibodies in solid tumors: direct experimental evidence for a binding site barrier.* Cancer Res, 1992. **52**(19): p. 5144-5153.
142. Adams, G.P., et al., *High affinity restricts the localization and tumor penetration of single-chain Fv antibody molecules.* Cancer Res, 2001. **61**(12): p. 4750-5.
143. Humm, J.L. and L.M. Cobb, *Nonuniformity of tumor dose in radioimmunotherapy.* J Nucl Med, 1990. **31**(1): p. 75-83.